J. Fluid Mech. (2000), *vol.* 423, *pp.* 345–380. Printed in the United Kingdom

© 2000 Cambridge University Press

On laminar separation at a corner point in transonic flow

By A. I. RUBAN AND I. TURKYILMAZ

Department of Mathematics, University of Manchester,
Oxford Road, Manchester M13 9PL, UK

(Received 26 May 1999 and in revised form 10 July 2000)

The separation of the laminar boundary layer from a convex corner on a rigid body contour in transonic flow is studied based on the asymptotic analysis of the Navier–Stokes equations at large values of the Reynolds number. It is shown that the flow in a small vicinity of the separation point is governed, as usual, by strong interaction between the boundary layer and the inviscid part of the flow. Outside the interaction region the Kármán–Guderley equation describing transonic inviscid flow admits a self-similar solution with the pressure on the body surface being proportional to the cubic root of the distance from the separation point. Analysis of the boundary layer driven by this pressure shows that as the interaction region is approached the boundary layer splits into two parts: the near-wall viscous sublayer and the main body of the boundary layer where the flow is locally inviscid. It is interesting that contrary to what happens in subsonic and supersonic flows, the displacement effect of the boundary layer is primarily due to the inviscid part. The contribution of the viscous sublayer proves to be negligible to the leading order. Consequently, the flow in the interaction region is governed by the *inviscid–inviscid interaction*. To describe this flow one needs to solve the Kármán–Guderley equation for the potential flow region outside the boundary layer; the solution in the main part of the boundary layer was found in an analytical form, thanks to which the interaction between the boundary layer and external flow can be expressed via the corresponding boundary condition for the Kármán–Guderley equation. Formulation of the interaction problem involves one similarity parameter which in essence is the Kármán–Guderley parameter suitably modified for the flow at hand. The solution of the interaction problem has been constructed numerically.

1. Introduction

The study of flow separation from the surface of a solid body, and the determination of global changes in the flow field that develop as a result of the separation, are among the most fundamental and difficult problems of fluid dynamics. It is well known that most liquid and gas flows observed in nature and encountered in engineering applications involve separation. In fact, to achieve an unseparated form of the flow past a rigid body at large values of the Reynolds number, rather severe restrictions must be imposed on the shape of the body.

Separation imposes a considerable limitation on the operating characteristics of aircraft wings, helicopter blades, turbines, etc., leading to a significant degradation of their performance. It is well known that the separation is normally accompanied by

a loss of the lift force, sharp increase of the drag, increase of the heat transfer at the reattachment region, pulsations of pressure and, as a result, flutter and buffet onset.

Modern asymptotic theory of boundary-layer separation is based on the so-called *triple-deck model* of the boundary-layer interaction with the inviscid part of the flow. It was formulated simultaneously by Neiland (1969) and Stewartson & Williams (1969) for the self-induced separation in supersonic flow and by Messiter (1970) for incompressible fluid flow near a trailing edge of a flat plate. Later it became clear that the triple-deck interaction region, although small, plays a key role in many fluid dynamic phenomena. It, for instance, governs upstream influence in supersonic boundary layers, development of different modes of instabilities, bifurcation of the solution and possible hysteresis of separated flows. As far as the separation phenomena are concerned, the theory has been extended to describe the boundary-layer separation from a smooth body surface in an incompressible fluid flow, supersonic flow separation provoked by a shock wave impinging upon the boundary layer, incipient and large-scale separations at angular points of the body contour both in subsonic and supersonic flows, separation at the trailing edge of a thin aerofoil appearing as a result of increase of the angle of attack or aerofoil thickness, leading-edge separation, separation of the boundary layer in hypersonic flow on a hot or cold wall, separation provoked by a wall roughness, etc. See Sychev *et al.* (1998) and references therein.

However, despite obvious progress in this field, many aspects of the boundary-layer separation theory remain unresolved. In particular, very little is still known about transonic flow separation. So far analysis of transonic viscous–inviscid interaction has been restricted to relatively simple situations when the flow outside the interaction region does not really show its transonic nature. To this category belongs, for example, the study of the flow near the trailing edge of a flat plate, performed by Bodonyi & Kluwick (1998). See also Bodonyi & Kluwick (1977, 1982) and Bodonyi (1979). In this problem the inviscid part of the flow remains uniform everywhere except in a small vicinity of the trailing edge, and the boundary layer on the plate surface is described by the compressible version of the Blasius solution. The interaction region, forming near the trailing edge, has conventional triple-deck structure, being composed of (i) the viscous near-wall sublayer, (ii) the main part of the boundary layer and (iii) the potential flow region outside the boundary layer. The interaction proceeds very much in the same way as in subsonic and supersonic flows, and may be described as follows.

In the viscous sublayer the fluid motion is relatively slow and for this reason the lower deck exhibits very high sensitivity to pressure variations. Even a small pressure rise along the wall may cause significant deceleration of fluid particles there. This leads to thickening of the flow filaments, and the streamlines change their shape, being displaced from the wall. The slope of the streamlines is then transmitted through the main part of the boundary layer to the potential flow in the upper deck. The potential flow performs the role of converting the perturbations of the slope into the perturbations of pressure. The latter, being transmitted back to the lower deck, cause thickening of the viscous sublayer, and the process repeats again. The middle deck plays a passive role in the interaction process. It does not contribute to the displacement effect of the boundary layer, and it does not change the pressure perturbations when transmitting them from the upper deck to the viscous sublayer.

The purpose of the present study is to demonstrate that the interaction process changes drastically when instead of the uniform flow outside the interaction region a real transonic flow separating from a rigid body surface is considered. It appears that the transonic flow separation is accompanied by a very strong pressure gradient acting upon the boundary layer upstream of the separation. This pressure gradient

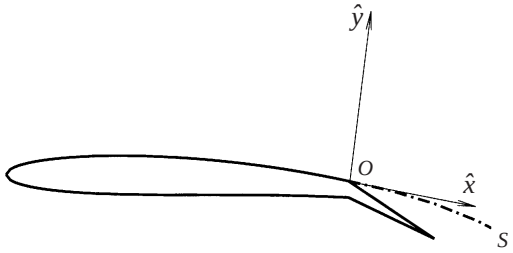

FIGURE 1. Flow past an aerofoil with the separation provoked by a deflected flap.

causes the velocity profile in the boundary layer to take a form which is significantly different to that in the subsonic or supersonic flows. For this reason the process of the interaction changes its nature and the flow is driven to separation by what may be referred to as the *inviscid–inviscid interaction.*

In the present paper our main attention is on the laminar boundary-layer separation at a corner point of a rigid body contour. The investigation of this flow is performed based on the asymptotic analysis of the Navier–Stokes equations at large values of the Reynolds number. It is shown that outside the interaction region the Kármán–Guderley equation, describing transonic inviscid flow, admits a self-similar solution. This solution predicts that the pressure on the body surface is proportional to the cubic root of the distance $-x$ from the separation point, and the pressure gradient $\mathrm{d}p/\mathrm{d}x \sim (-x)^{-2/3}$. The analysis of the boundary layer driven by this pressure gradient reveals that, as the interaction region is approached, the boundary layer splits into two parts: the near-wall viscous sublayer whose thickness may be estimated as $y \sim Re^{-1/2}(-x)^{5/12}$, and the main body of the boundary layer where the flow is locally inviscid. It is remarkable that contrary to what happens in subsonic and supersonic flows, the displacement effect of the boundary layer is primarily due to the inviscid part. The contribution of the viscous sublayer proves to be negligible to the leading order. Consequently, the flow in the interaction region, which forms near the angular point, is governed by the inviscid–inviscid interaction. The longitudinal extent of this region is estimated as $\Delta x = O(Re^{-3/7})$.

To describe the flow in the interaction region one needs to solve the Kármán–Guderley equation for the potential flow outside the boundary layer; the solution in the main part of the boundary layer was found in an analytical form, thanks to which the interaction between the boundary layer and external flow can be expressed via the corresponding boundary condition for the Kármán–Guderley equation. Formulation of the interaction problem involves one similarity parameter which in essence is the Kármán–Guderley parameter suitably modified for the flow at hand. The solution of the interaction problem has been constructed numerically.

2. Inviscid flow outside the interaction region

Consider two-dimensional flow of a perfect gas past a rigid body with separation at an angular point of the body contour. An example is the flow over an aerofoil with a flap deflected through an angle which is assumed sufficiently large to cause flow separation at angular point O as shown in figure 1. Let us further assume that the separation region is much longer than the region of interaction we anticipate to form in a small vicinity of point O. In this case the high Reynolds number limit of the solution of the governing Navier–Stokes equations is represented by the inviscid flow

in which the shear layer developing along the separation streamline OS degenerates into a line of discontinuity of the tangential velocity. In what follows this line will be referred to as the free streamline.

It is well known that any two-dimensional steady flow of a perfect gas may be described by the following equation:

$$(\hat{a}^2 - \hat{u}^2)\frac{\partial \hat{u}}{\partial \hat{x}} + (\hat{a}^2 - \hat{v}^2)\frac{\partial \hat{v}}{\partial \hat{y}} = \hat{u}\hat{v}\left(\frac{\partial \hat{v}}{\partial \hat{x}} + \frac{\partial \hat{u}}{\partial \hat{y}}\right). \tag{2.1}$$

Here $\hat{x}$, $\hat{y}$ are Cartesian coordinates and $\hat{u}$, $\hat{v}$ are velocity components with respect to these coordinates. For our purposes it is convenient to choose the coordinate system in such a way that its origin coincides with angular point O and the $\hat{x}$-axis is directed along the tangent to the body surface upstream of the separation.

The speed of sound is denoted in equation (2.1) by $\hat{a}$. Its value at each point of the flow field is related to the velocity components via the Bernoulli's equation

$$\frac{\hat{a}^2}{\gamma - 1} + \frac{\hat{u}^2 + \hat{v}^2}{2} = \frac{\hat{a}_\infty^2}{\gamma - 1} + \frac{\hat{V}_\infty^2}{2}, \tag{2.2}$$

where γ is the specific heat ratio, $\hat{V}_\infty$ is the gas velocity in unperturbed flow far upstream of the aerofoil and $\hat{a}_\infty$ denotes the corresponding value of the speed of sound.

If the flow is free of shock waves, or shock waves are weak, which always is the case in transonic flows, then the flow may be treated as irrotational (see Appendix A), and there exists the potential function $\hat{\Phi}(\hat{x}, \hat{y})$ such that

$$\hat{u} = \frac{\partial \hat{\Phi}}{\partial \hat{x}}, \quad \hat{v} = \frac{\partial \hat{\Phi}}{\partial \hat{y}}. \tag{2.3}$$

Once the solution of equations (2.1)–(2.3) is found, one can determine the pressure $\hat{p}$ and density $\hat{\rho}$ at each point of the flow field using Bernoulli's equation (2.2), written in the form, where the well known formula for the speed of sound $\hat{a}^2 = \gamma \hat{p}/\hat{\rho}$ is used,

$$\frac{\gamma}{\gamma - 1}\frac{\hat{p}}{\hat{\rho}} + \frac{\hat{u}^2 + \hat{v}^2}{2} = \frac{\gamma}{\gamma - 1}\frac{\hat{p}_\infty}{\hat{\rho}_\infty} + \frac{\hat{V}_\infty^2}{2}, \tag{2.4}$$

and the entropy conservation law

$$\frac{\hat{p}}{\hat{\rho}^\gamma} = \frac{\hat{p}_\infty}{\hat{\rho}_\infty^\gamma}. \tag{2.5}$$

In this study the pressure everywhere in the separation region and, in particular, along the free streamline OS is assumed constant. Its value will be denoted as $\hat{p}_s$. By Bernoulli's theorem and the entropy conservation law the flow velocity $\hat{V}_s$, speed of sound $\hat{a}_s$ and gas density $\hat{\rho}_s$ should also remain constant on the free streamline. Using these quantities we can introduce non-dimensional variables as follows:

$$\left.\begin{array}{c} \hat{u} = \hat{V}_s u, \quad \hat{v} = \hat{V}_s v, \quad \hat{\Phi} = \hat{V}_s L \Phi, \\ \hat{a} = \hat{V}_s a, \quad \hat{\rho} = \hat{\rho}_s \rho, \quad \hat{p} = \hat{p}_s + \hat{\rho}_s \hat{V}_s^2 p, \\ \hat{x} = Lx, \quad \hat{y} = Ly, \end{array}\right\} \tag{2.6}$$

where L is the characteristic dimension of the body.

Substitution of (2.6) into (2.1)–(2.3) gives

$$(a^2 - u^2)\frac{\partial u}{\partial x} + (a^2 - v^2)\frac{\partial v}{\partial y} = uv\left(\frac{\partial v}{\partial x} + \frac{\partial u}{\partial y}\right), \tag{2.7}$$

$$u = \frac{\partial \Phi}{\partial x}, \quad v = \frac{\partial \Phi}{\partial y}, \tag{2.8}$$

$$\frac{a^2}{\gamma - 1} + \frac{u^2 + v^2}{2} = \frac{1}{(\gamma - 1)M_s^2} + \frac{1}{2}, \tag{2.9}$$

where M_s is the value of the Mach number on the free streamline OS:

$$M_s = \frac{\hat{V}_s}{\hat{a}_s}.$$

Bernoulli's equation (2.4) and the entropy conservation law (2.5) written in the non-dimensional variables take the form

$$\frac{u^2 + v^2}{2} + \frac{1}{(\gamma - 1)M_s^2 \rho} + \frac{\gamma}{\gamma - 1}\frac{p}{\rho} = \frac{1}{2} + \frac{1}{(\gamma - 1)M_s^2}, \tag{2.10}$$

$$1 + \gamma M_s^2 p = \rho^\gamma. \tag{2.11}$$

To formulate boundary conditions which should be applied when solving equations (2.7)–(2.9) we represent the body contour upstream of the separation point as

$$y = Y_b(x), \quad x < 0,$$

while for the free streamline OS we will use the equation

$$y = Y_s(x), \quad x > 0.$$

Here function $Y_s(x)$ should be found as a part of the solution of the problem. The impermeability condition on the body surface upstream of the separation may be written as

$$\frac{v}{u} = Y_b'(x) \quad \text{at} \quad y = Y_b(x), \quad x < 0. \tag{2.12}$$

Downstream of the separation point the conditions for the pressure

$$p = 0 \quad \text{at} \quad y = Y_s(x), \quad x > 0 \tag{2.13}$$

and the free-streamline slope

$$\frac{v}{u} = Y_s'(x) \quad \text{at} \quad y = Y_s(x), \quad x > 0 \tag{2.14}$$

should hold.

We shall now suppose that the Mach number on the free streamline is

$$M_s = 1 + \epsilon M_1, \tag{2.15}$$

where M_1 is an order-one constant and ϵ is a small parameter which will be determined later. The solution of the problem formulated above will be sought in the form of the straightforward asymptotic expansions

$$\left.\begin{aligned} u &= u_0(x,y) + \epsilon u_1(x,y) + \cdots, & v &= v_0(x,y) + \epsilon v_1(x,y) + \cdots, \\ \Phi &= \Phi_0(x,y) + \epsilon \Phi_1(x,y) + \cdots, & a &= a_0(x,y) + \epsilon a_1(x,y) + \cdots, \\ p &= p_0(x,y) + \epsilon p_1(x,y) + \cdots, & \rho &= \rho_0(x,y) + \epsilon \rho_1(x,y) + \cdots, \\ Y_s &= Y_0(x) + \epsilon Y_1(x) + \cdots. \end{aligned}\right\} \tag{2.16}$$

2.1. *Leading-order solution in the physical plane*

Substitution of (2.16) together with (2.15) into (2.7)–(2.9) yields to the leading order

$$(a_0^2 - u_0^2)\frac{\partial u_0}{\partial x} + (a_0^2 - v_0^2)\frac{\partial v_0}{\partial y} = 2u_0 v_0 \frac{\partial u_0}{\partial y}, \tag{2.17}$$

$$u_0 = \frac{\partial \Phi_0}{\partial x}, \quad v_0 = \frac{\partial \Phi_0}{\partial y}, \tag{2.18}$$

$$\frac{a_0^2}{\gamma - 1} + \frac{u_0^2 + v_0^2}{2} = \frac{\gamma + 1}{2(\gamma - 1)}. \tag{2.19}$$

From boundary conditions (2.12)–(2.14) it follows that

$$v_0 = Y_b'(x)u_0 \quad \text{at} \quad y = Y_b(x), \quad x < 0 \tag{2.20}$$

and

$$\left.\begin{array}{l} p_0 = 0 \\ v_0 = Y_0'(x)\, u_0 \end{array}\right\} \quad \text{at} \quad y = Y_0(x), \quad x > 0, \tag{2.21}$$

while Bernoulli's equation (2.10) and the entropy conservation law (2.11) reduce to

$$\frac{u_0^2 + v_0^2}{2} + \frac{1}{(\gamma - 1)\rho_0} + \frac{\gamma}{\gamma - 1}\frac{p_0}{\rho_0} = \frac{\gamma + 1}{2(\gamma - 1)}, \tag{2.22}$$

$$1 + \gamma p_0 = \rho_0^{\gamma}. \tag{2.23}$$

This completes formulation of the leading-order problem.

Taking into account that no length scale can be ascribed to the body shape in a small vicinity of the angular point O, we shall seek a 'local' solution of problem (2.17)–(2.23) near point O in a self-similar form. For the velocity potential $\Phi_0(x, y)$ the following coordinate expansion will be used:

$$\Phi_0(x, y) = x + \frac{1}{\gamma + 1} y^{3k-2} F_0(\xi) + \cdots \quad \text{as} \quad y \to 0, \tag{2.24}$$

where the independent variable

$$\xi = \frac{x}{y^k} \tag{2.25}$$

is supposed to remain an order-one quantity as x and y simultaneously tend to zero. This is only possible if parameter k is positive.

Using (2.18) and then Bernoulli's equation (2.19) it may be easily found that

$$u_0 = 1 + \frac{1}{\gamma + 1} y^{2k-2} F_0'(\xi) + \cdots, \tag{2.26}$$

$$v_0 = \frac{1}{\gamma + 1} y^{3k-3} [(3k - 2)F_0(\xi) - k\xi F_0'(\xi)] + \cdots, \tag{2.27}$$

$$a_0 = 1 - \frac{(\gamma - 1)}{2(\gamma + 1)} y^{2k-2} F_0'(\xi) + \cdots. \tag{2.28}$$

Since the velocity vector at the separation point should be tangent to the body contour and its modulus should tend to unity as $y \to 0$, we have to impose upon parameter k an additional restriction $k > 1$.

Substitution of (2.26)–(2.28) into (2.17) results in the following equation for function $F_0(\xi)$:

$$(F_0' - k^2\xi^2)F_0'' - k(5-5k)\xi F_0' + (3-3k)(3k-2)F_0 = 0. \tag{2.29}$$

This equation has been studied extensively with the purpose of describing the 'far field' behaviour of the transonic flows past an aerofoil.† Among publications on this topic see Guderley & Yoshihara (1951), Guderley (1962), Falkovich & Chernov (1964) and the more recent book by Cole & Cook (1986).

Boundary conditions for (2.29) may be formulated in the following way. Near the body surface upstream of the separation point O, where ξ is large and negative, an asymptotic expansion of function $F_0(\xi)$ is sought in the form

$$F_0(\xi) = d\,(-\xi)^{\alpha} + \cdots \quad \text{as} \quad \xi \to -\infty. \tag{2.30}$$

Substituting (2.30) into equation (2.29) it is easily found that if $\alpha < 3$, then

$$-k^2\alpha(\alpha-1) - k(5-5k)\alpha + (3-3k)(3k-2) = 0, \tag{2.31}$$

with the coefficient d remaining arbitrary.

Quadratic equation (2.31) has two solutions

$$\alpha_1 = 3 - \frac{2}{k}, \quad \alpha_2 = 3 - \frac{3}{k}$$

both satisfying the condition $\alpha < 3$. Hence

$$F_0(\xi) = d_0(-\xi)^{3-2/k} + d_1(-\xi)^{3-3/k} + \cdots \quad \text{as} \quad \xi \to -\infty. \tag{2.32}$$

Substitution of (2.32) into (2.27) results in

$$v_0 = \frac{d_1}{\gamma+1}(-x)^{3-3/k} + \cdots \quad \text{as} \quad x \to 0^-. \tag{2.33}$$

Suppose, subject to subsequent confirmation, that $k < 3/2$. Suppose further that the curvature of the body contour just upstream of the separation point is finite, i.e $Y_b = O\left[(-x)^2\right]$ as $x \to 0^-$. Then using (2.33) and (2.26) in the impermeability condition (2.20) we see that the second coefficient d_1 in expansion (2.32) should be set to zero:

$$d_1 = 0. \tag{2.34}$$

To apply boundary conditions (2.21), a formula representing the asymptotic behaviour of the pressure near the angular point is needed. It may be derived by substituting (2.26), (2.27) into equations (2.22), (2.23) and solving these equations for p_0 and ρ_0. As a result we find

$$p_0(x,y) = -\frac{1}{\gamma+1}y^{2k-2}F_0'(\xi) + \cdots, \tag{2.35}$$

$$\rho_0(x,y) = 1 - \frac{1}{\gamma+1}y^{2k-2}F_0'(\xi) + \cdots$$

as $y \to 0$ and $\xi = O(1)$.

Similarly to (2.32), it may be shown that at large positive values of ξ

$$F_0(\xi) = b_0\xi^{3-2/k} + b_1\xi^{3-3/k} + \cdots \quad \text{as} \quad \xi \to +\infty. \tag{2.36}$$

† To use expansions (2.26)–(2.28) for large values of y one needs to restrict parameter k to the interval $0 < k < 1$.

Substitution of (2.36) into (2.26), (2.27) and (2.35) gives

$$u_0 = 1 + \frac{1}{\gamma+1}\left[b_0\left(3-\frac{2}{k}\right)x^{2-2/k} + b_1\left(3-\frac{3}{k}\right)yx^{2-3/k} + \cdots\right], \tag{2.37}$$

$$v_0 = \frac{1}{\gamma+1}b_1x^{3-3/k} + \cdots, \tag{2.38}$$

$$p_0 = -\frac{1}{\gamma+1}\left[b_0\left(3-\frac{2}{k}\right)x^{2-2/k} + b_1\left(3-\frac{3}{k}\right)yx^{2-3/k} + \cdots\right]. \tag{2.39}$$

Using (2.37) and (2.38) in the second of boundary conditions (2.21) the formula

$$Y_0(x) = \frac{b_1}{\gamma+1}\,\frac{1}{4-3/k}x^{4-3/k} + \cdots \quad \text{as} \quad x \to 0^+$$

representing the form of the free streamline, may be derived. Using this formula it is easily verified that on the free streamline, where $y = Y_0(x)$, the second term in (2.39) is small compared with the first one. Hence, to satisfy the first of boundary conditions (2.21) one needs to set

$$b_0 = 0. \tag{2.40}$$

Equation (2.29) considered with boundary conditions (2.34) and (2.40) constitutes a nonlinear eigenvalue problem which if solved determines parameter k. To study this problem we notice that equation (2.29) admits the invariant transformation

$$F_0(\xi) = C^3F_0(\xi/C),$$

with C being an arbitrary constant. This means that without loss of generality one can choose the first coefficient d_0 in (2.32) to be $d_0 = 1$ for all positive d_0, and $d_0 = -1$ for all negative d_0. In this presentation we will concentrate on the former case for the following reason. Substitution of (2.32) into (2.26) yields to the leading order

$$u_0 = 1 - \frac{d_0}{\gamma+1}\left(3-\frac{2}{k}\right)(-x)^{2-2/k} + \cdots \quad \text{as} \quad x \to 0^-.$$

This shows that with a positive value of d_0 the flow experiences acceleration before separation, which is typical of separation from angular points.

Taking into account that in view of condition (2.34) the second term in (2.32) should be omitted, and calculating the next-order term we have

$$F_0(\xi) = (-\xi)^{3-2/k} + \frac{(3k-2)^2(1-k)}{k^3}(-\xi)^{3-4/k} + \cdots \quad \text{as} \quad \xi \to -\infty.$$

This formula was used in our calculations to determine initial conditions for F_0 and F_0' at the left-hand-side boundary $\xi = \xi_{\min}$ of the computational domain $\xi \in [\xi_{\min}, \xi_{\max}]$. Equation (2.29) was then integrated numerically from $\xi = \xi_{\min}$ towards $\xi = \xi_{\max}$ for different values of parameter k. The Runge–Kutta fourth-order method was employed for this purpose. A number of computational domains were tried, the largest being $[-50, 50]$. A uniform mesh was used throughout this analysis with up to 2000 node points between $\xi = \xi_{\min}$ and $\xi = \xi_{\max}$. The results proved to be mesh independent, and are presented in figure 2 where the graphs of derivative F_0' against ξ are plotted.

As follows from asymptotic formula (2.36)

$$F_0' = b_0\left(3-\frac{2}{k}\right)\xi^{2-2/k} + \cdots \quad \text{as} \quad \xi \to +\infty.$$

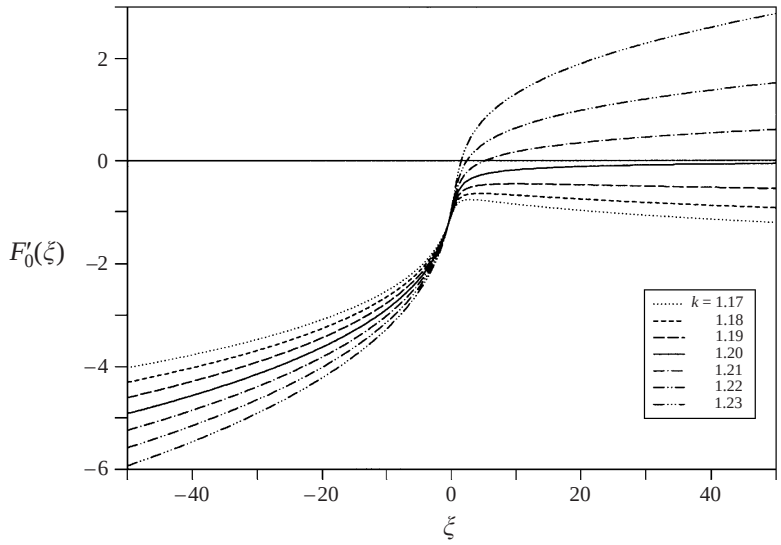

FIGURE 2. Results of the numerical solution of equation (2.29).

Thus $|F_0'(\xi)|$ proves to grow with ξ for all $k > 1$, unless $b_0 = 0$. Taking this into account and observing the behaviour of $F_0'(\xi)$ in figure 2, it may be seen that to satisfy boundary condition (2.40) one has to choose

$$k = \tfrac{6}{5}.$$

This result was earlier reported by Diesperov (1994) who performed his analysis based on the transonic small perturbation theory in which case the hodograph method may be applied.

2.2. *Hodograph method*

Suppose that the aerofoil is thin and the separation region is shallow, i.e.

$$Y_b(x) = \delta \tilde{Y}_b(x), \quad Y_0(x) = \delta \tilde{Y}_0(x),$$

where δ is a small positive parameter, and $\tilde{Y}_b(x)$, $\tilde{Y}_0(x)$ are order-one functions. Then the solution of the leading-order problem (2.17)–(2.19) may be sought using the following asymptotic expansion for the potential:

$$\Phi_0(x, y; \delta) = x + \delta^{2/3}\phi_0(x, \tilde{y}) + \cdots, \tag{2.41}$$

where

$$\tilde{y} = \delta^{1/3} y.$$

Differentiating (2.41) in accordance with (2.18) we have

$$u_0 = 1 + \delta^{2/3}\frac{\partial \phi_0}{\partial x} + \cdots, \quad v_0 = \delta \frac{\partial \phi_0}{\partial \tilde{y}} + \cdots, \tag{2.42}$$

and then using Bernoulli's equation (2.19) we can find that

$$a_0^2 = 1 - \delta^{2/3}(\gamma - 1)\frac{\partial \phi_0}{\partial x} + \cdots. \tag{2.43}$$

Substitution of (2.42), (2.43) into (2.17) leads to the Kármán–Guderley equation

$$(\gamma+1)\frac{\partial\phi_0}{\partial x}\frac{\partial^2\phi_0}{\partial x^2}-\frac{\partial^2\phi_0}{\partial\tilde{y}^2}=0. \tag{2.44}$$

Once this equation is solved, the pressure distribution over the flow field may be found by making use of the formula

$$p_0=-\delta^{2/3}\frac{\partial\phi_0}{\partial x}+\cdots, \tag{2.45}$$

which is easily derived from equations (2.22), (2.23) using (2.42).

Solution of the Kármán–Guderley equation (2.44) may be sought, as before, in the form

$$\phi_0(x,\tilde{y})=\frac{1}{\gamma+1}\tilde{y}^{3k-2}F_0(\xi),\quad \xi=\frac{x}{\tilde{y}^k},$$

which leads to equation (2.29). Alternatively the hodograph method may be used. For this purpose we write equation (2.44) as

$$w\frac{\partial w}{\partial x}-\frac{\partial\vartheta}{\partial\tilde{y}}=0,\quad \frac{\partial w}{\partial\tilde{y}}-\frac{\partial\vartheta}{\partial x}=0, \tag{2.46}$$

where

$$w=(\gamma+1)\frac{\partial\phi_0}{\partial x},\quad \vartheta=(\gamma+1)\frac{\partial\phi_0}{\partial\tilde{y}}, \tag{2.47}$$

and then, on changing the roles of the dependent and independent variables, equations (2.46) become

$$w\frac{\partial\tilde{y}}{\partial\vartheta}-\frac{\partial x}{\partial w}=0,\quad \frac{\partial\tilde{y}}{\partial w}-\frac{\partial x}{\partial\vartheta}=0. \tag{2.48}$$

Function $x(w,\vartheta)$ may be excluded from these equations by cross-differentiation. The resulting equation for $\tilde{y}(w,\vartheta)$ is

$$w\frac{\partial^2\tilde{y}}{\partial\vartheta^2}-\frac{\partial^2\tilde{y}}{\partial w^2}=0. \tag{2.49}$$

The self-similar solution of equation (2.49) has the form

$$\tilde{y}(w,\vartheta)=\vartheta^n f(\zeta),\quad \zeta=\frac{w}{\vartheta^{2/3}}. \tag{2.50}$$

To find the relationship between parameter n in the self-similar solution (2.50) in the hodograph plane and parameter k in the self-similar solution (2.24) in the physical plane, we notice, based on (2.50) and either of the equations (2.48), that $x(w,\vartheta)$ should be written as

$$x(w,\vartheta)=\vartheta^{n+1/3}g(\zeta).$$

Consequently,

$$\xi=\frac{x}{\tilde{y}^k}=\vartheta^{1/3-n(k-1)}\frac{g(\zeta)}{\big[f(\zeta)\big]^k}.$$

Setting the exponent of ϑ in this formula to zero, we have

$$k=1+\frac{1}{3n}. \tag{2.51}$$

Substitution of (2.50) into (2.49) results in the following equation for function $f(\zeta)$:

$$\big(1-\tfrac{4}{9}\zeta^3\big)f''+\tfrac{2}{3}\big(2n-\tfrac{5}{3}\big)\zeta^2 f'-n(n-1)\zeta f=0. \tag{2.52}$$

Representing $f(\zeta)$ in the form

$$f(\zeta) = z^{-n/2}A(z), \quad z = \frac{1}{1-\frac{4}{9}\zeta^3} \tag{2.53}$$

reduces (2.52) to the hypergeometric equation (see, for example, Abramowitz & Stegun 1965)

$$z(1-z)\frac{\mathrm{d}^2A}{\mathrm{d}z^2} + \left(\tfrac{1}{2} - \tfrac{7}{6}z\right)\frac{\mathrm{d}A}{\mathrm{d}z} + \tfrac{1}{4}n\left(n+\tfrac{1}{3}\right)A = 0, \tag{2.54}$$

its parameters being

$$a = \tfrac{1}{6} + \tfrac{1}{2}n, \quad b = -\tfrac{1}{2}n, \quad c = \tfrac{1}{2}.$$

It is well known that two complementary solutions of the hypergeometric equation may be chosen to be

$$A_1(z) = F(a,b;c;z),$$
$$A_2(z) = z^{1-c}F(a-c+1, b-c+1; 2-c; z),$$

where $F(a,b;c;z)$ is the hypergeometric function defined inside the circle $|z| < 1$ by the Gauss series

$$F(a,b;c;z) = 1 + \frac{ab}{c}z + \frac{a(a+1)b(b+1)}{c(c+1)}\frac{z^2}{2!} + \cdots.$$

Thus the general solution of equation (2.54) is written as

$$A(z) = C_1F\left(\tfrac{1}{6} + \tfrac{1}{2}n, -\tfrac{1}{2}n; \tfrac{1}{2}; z\right) + C_2\, z^{1/2}F\left(\tfrac{2}{3} + \tfrac{1}{2}n, \tfrac{1}{2} - \tfrac{1}{2}n; \tfrac{3}{2}; z\right). \tag{2.55}$$

Let us now consider the boundary conditions on the aerofoil surface upstream of the separation point and on the free streamline downstream of the separation (see figure 3). Above the aerofoil surface the flow is subsonic $w < 0$, and it accelerates towards the separation point, which means that $\vartheta < 0$. As the wall is approached, ϑ tends to zero and ζ becomes infinitely large according to (2.50). Using (2.53) we see that z tends to zero as

$$z = \tfrac{9}{4}(-\zeta)^{-3} + \cdots. \tag{2.56}$$

Substitution of (2.56) into (2.53) and then into (2.50) results in

$$\tilde{y} = \left(\tfrac{2}{3}\right)^n(-w)^{3n/2}A(z) + \cdots.$$

Taking into account that on the aerofoil surface $\tilde{y} = 0$, we have to conclude that $A(0) = 0$ which is only possible if C_1 in (2.55) is zero.

Turning to the boundary condition on the free streamline, we set $w = 0$ which gives $\zeta = 0$ and $z = 1$. Substitution of (2.53) into (2.50) yields

$$\tilde{y} = \vartheta^n A(z) + \cdots,$$

and since on the free streamline $\tilde{y} = 0$, we have to conclude that

$$A(1) = 0. \tag{2.57}$$

Choosing $z = 1$ in (2.55) and taking into account that†

$$F(a,b;c;1) = \frac{\Gamma(c)\Gamma(c-a-b)}{\Gamma(c-a)\Gamma(c-b)},$$

† This formula may be used if $c \neq 0, -1, -2, \ldots$, and $c - a - b > 0$.

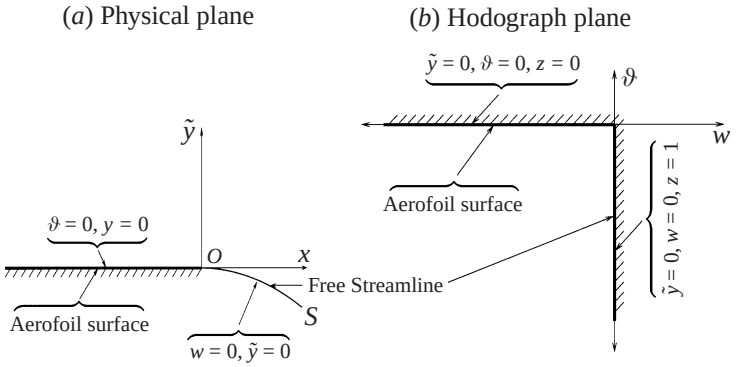

FIGURE 3. Boundary conditions in the physical and hodograph planes.

leads to

$$A(1) = C_2 \frac{\Gamma(3/2)\Gamma(1/3)}{\Gamma(5/6 - n/2)\Gamma(1 + n/2)}. \tag{2.58}$$

Thus boundary condition (2.57) may be satisfied only if one of the gamma-functions in the denominator in (2.58) may be made infinite. Since n is positive, $\Gamma(1 + n/2)$ always stays finite. $\Gamma(5/6 - n/2)$ becomes infinite if the argument $5/6 - n/2$ is zero or assumes a negative integer value. This yields the following set of eigenvalues:

$$n = \tfrac{5}{3} + 2l, \quad l = 0, 1, 2, \ldots .$$

The corresponding eigenfunctions may be easily studied by means of direct numerical solution of equation (2.54). The results of the calculations are presented in figure 4, which shows that all the eigenfunctions, except the first one, are sign-alternating and cannot be used to describe a real flow. Indeed, it follows from (2.50) and (2.53) that $A(z)$ is proportional to $\tilde{y}$, the latter being strictly positive in the flow considered. For this reason we will restrict our attention to the first eigenvalue

$$n = \tfrac{5}{3}. \tag{2.59}$$

Substitution of (2.59) into (2.51) confirms that parameter k in the self-similar solution (2.24) in the physical plane should be taken $k = 6/5$.

With this particular value of parameter n the solution may be simplified using the identity

$$F(a, b; c; z) = (1 - z)^{c-a-b} F(c - a, c - b; c; z),$$

which reduces (2.55) to

$$A(z) = C_2 z^{1/2} (1 - z)^{1/3}. \tag{2.60}$$

Substituting (2.60) back into (2.53) and then into (2.50) we find that the solution of equation (2.49) has the remarkably simple form

$$\tilde{y} = Cw\vartheta. \tag{2.61}$$

Here constant $C = -(2/3)^{2/3} C_2$ remains arbitrary from the standpoint of the 'local' flow analysis. It is, however, expected to be determined uniquely if the 'global' solution of the problem is found.

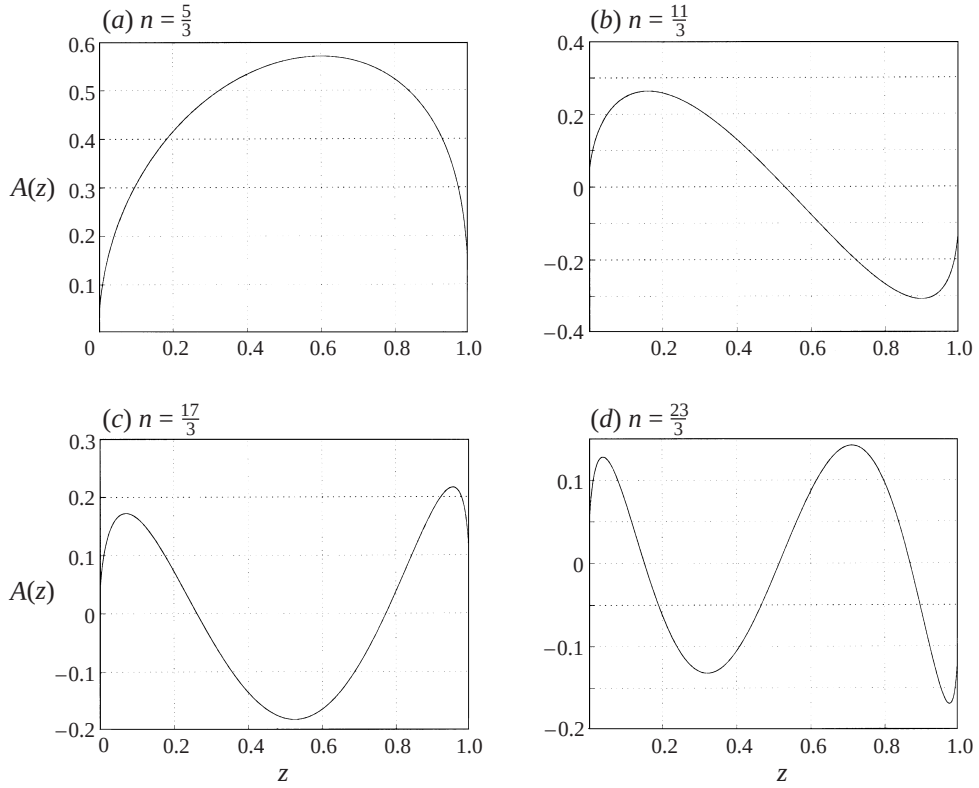

FIGURE 4. The first four eigenfunctions.

Finally, making use of equations (2.48) we have

$$x = \tfrac{1}{3}Cw^3 + \tfrac{1}{2}C\vartheta^2. \tag{2.62}$$

Let us, first, apply this equation to the flow on the aerofoil surface upstream of the separation. Here $\vartheta = 0$, and we have

$$w = -\left(\frac{3}{C}\right)^{1/3}(-x)^{1/3}. \tag{2.63}$$

Since upstream of the separation both w and x are negative, constant C should be positive. Combining (2.63) with (2.45) and (2.47) leads to the following formula for the pressure on the aerofoil surface:

$$p_0(x) = \frac{N}{\gamma+1}(-x)^{1/3} + \cdots \quad \text{as} \quad x \to 0^-. \tag{2.64}$$

Here constant $N = (3\delta^2/C)^{1/3}$ is positive and does not depend on the Reynolds number, which is why in what follows N will be assumed an order-one quantity.

Let us now consider the free streamline. Setting $w = 0$ in (2.62) we have

$$\vartheta = -\sqrt{\frac{2}{C}}x^{1/2}.$$

Then using further equations (2.47), (2.42) and the second boundary condition in

(2.21) we arrive at the formula

$$Y_0(x) = -\frac{1}{\gamma+1}\left(\tfrac{2}{3}N\right)^{3/2}x^{3/2} + \cdots \quad \text{as} \quad x \to 0^+ \tag{2.65}$$

which defines the shape of the free streamline.

2.3. *Next-order approximation*

We now return to asymptotic expansions (2.16) and consider the perturbations caused by small variations ϵM_1 of the Mach number (2.15). Substituting (2.15), (2.16) into (2.7)–(2.9) and collecting $O(\epsilon)$ terms leads to the following set of equations:

$$(a_0^2 - u_0^2)\frac{\partial u_1}{\partial x} + 2\frac{\partial u_0}{\partial x}(a_0a_1 - u_0u_1) + (a_0^2 - v_0^2)\frac{\partial v_1}{\partial y} + 2\frac{\partial v_0}{\partial y}(a_0a_1 - v_0v_1)$$
$$= 2u_0v_0\frac{\partial u_1}{\partial y} + 2\frac{\partial u_0}{\partial y}(u_0v_1 + v_0u_1), \tag{2.66}$$

$$u_1 = \frac{\partial \Phi_1}{\partial x}, \quad v_1 = \frac{\partial \Phi_1}{\partial y}, \tag{2.67}$$

$$\frac{2a_0a_1}{\gamma-1} + u_0u_1 + v_0v_1 = -\frac{2M_1}{\gamma-1}. \tag{2.68}$$

From boundary conditions (2.12)–(2.14) it follows that

$$v_1 = Y_b'u_1 \quad \text{at} \quad y = Y_b(x), \quad x < 0 \tag{2.69}$$

and

$$\left.\begin{aligned} p_1 &= -Y_1\frac{\partial p_0}{\partial y} \\ v_1 &= -Y_1\frac{\partial v_0}{\partial y} + Y_1'u_0 + Y_0'\left(u_1 + Y_1\frac{\partial u_0}{\partial y}\right) \end{aligned}\right\} \quad \text{at} \quad y = Y_0(x), \quad x > 0, \tag{2.70}$$

while the Bernoulli's equation (2.10) and entropy conservation law (2.11) yield

$$u_0u_1 + v_0v_1 - \frac{2M_1}{(\gamma-1)\rho_0} - \frac{\rho_1}{(\gamma-1)\rho_0^2} + \frac{\gamma}{\gamma-1}\left(\frac{p_1}{\rho_0} - \frac{p_0\rho_1}{\rho_0^2}\right) = -\frac{2M_1}{\gamma-1}, \tag{2.71}$$

$$\gamma p_1 + 2\gamma M_1 p_0 = \gamma\rho_0^{\gamma-1}\rho_1. \tag{2.72}$$

Solution of boundary-value problem (2.66)–(2.72) may be sought near the separation point in the form

$$\Phi_1(x,y) = \frac{1}{\gamma+1}y^\alpha F_1(\xi) + \cdots \quad \text{as} \quad y \to 0, \tag{2.73}$$

with the independent variable being again

$$\xi = \frac{x}{y^k}.$$

Substitution of (2.73) into (2.66)–(2.68) leads to the following equation for $F_1(\xi)$:

$$(F_0' - k^2\xi^2)F_1'' + \left[F_0'' + k(2\alpha - k - 1)\xi\right]F_1' - \alpha(\alpha-1)F_1 = -2M_1F_0''\Delta_{\alpha,k}, \tag{2.74}$$

where

$$\Delta_{\alpha,k} = \begin{cases} 0 & \text{if} \quad \alpha \neq k \\ 1 & \text{if} \quad \alpha = k. \end{cases}$$

Near the aerofoil surface upstream of the separation point the solution of equation (2.74) may be represented by the asymptotic expansion

$$F_1(\xi) = r_0(-\xi)^{\alpha/k} + r_1(-\xi)^{(\alpha-1)/k} + O\left[(-\xi)^{(\alpha-2)/k}\right] \quad \text{as} \quad \xi \to -\infty. \tag{2.75}$$

Substitution of (2.75) into (2.73) and (2.67) and then into boundary condition (2.69) shows that the second constant in (2.75) should be set to zero:

$$r_1 = 0.$$

Similarly, near the free streamline downstream of the separation, solution of equation (2.74) may be written in the form

$$F_1(\xi) = q_0\xi^{\alpha/k} + q_1\xi^{(\alpha-1)/k} + O[\xi^{(\alpha-2)/k}] \quad \text{as} \quad \xi \to +\infty. \tag{2.76}$$

Substituting (2.76) into (2.73) and (2.67) and then into the Bernoulli's equation (2.71) and entropy conservation law (2.72) one can find that

$$\left.\begin{aligned} u_1 &= \frac{q_0}{\gamma+1}\frac{\alpha}{k}x^{(\alpha-k)/k} + \cdots \\ v_1 &= \frac{q_1}{\gamma+1}x^{(\alpha-1)/k} + \cdots \\ p_1 &= -\frac{q_0}{\gamma+1}\frac{\alpha}{k}x^{(\alpha-k)/k} + \cdots \end{aligned}\right\} \quad \text{as} \quad x \to 0^+.$$

Using these expressions in (2.70) leads to a conclusion that the second boundary condition for equation (2.74) is

$$q_0 = 0.$$

We now are in a position to claim that the power α in (2.73) should be chosen to be $\alpha = k$. Indeed, perturbations to the leading-order approximation in (2.16) are supposed to appear as a consequence of the variation ϵM_1 of the Mach number (2.15). However, unless $\alpha = k$ equation (2.74) for $F_1(\xi)$ and the corresponding boundary conditions do not involve M_1.

Setting $\alpha = k$ and substituting (2.73) and (2.24) into the expansion of the potential Φ in (2.16) leads to

$$\Phi = x + \frac{1}{\gamma+1}y^{8/5}F_0(\xi) + \frac{\epsilon}{\gamma+1}y^{6/5}F_1(\xi) + \cdots, \tag{2.77}$$

and we see that the solution based on asymptotic expansions (2.16) does not remain uniformly valid in a small vicinity of the separation point. Indeed, once y becomes as small as

$$y \sim \epsilon^{5/2} \tag{2.78}$$

the third and second terms in (2.77) become of the same order of magnitude, and expansions (2.16) can no longer be used. To find the longitudinal extent of the region of non-uniformity, the form of the similarity variable (2.25) should be taken into account. For ξ to stay an order-one quantity we need to choose

$$x \sim y^{6/5} \sim \epsilon^3. \tag{2.79}$$

We will suppose in this study that the region of non-uniformity coincides with the upper deck of the interactions region, which will be analysed §4.

3. Boundary layer upstream of the interaction region

To describe the flow in the boundary layer on the aerofoil surface upstream of the separation we will use orthogonal curvilinear coordinates $\hat{x}'$, $\hat{y}'$ where $\hat{x}'$ is measured along the aerofoil contour and $\hat{y}'$ in the perpendicular direction. The velocity components in these coordinates will be denoted by $\hat{u}'$ and $\hat{v}'$. The pressure and gas density are denoted as before by $\hat{p}$ and $\hat{\rho}$. In the boundary layer we also need to consider the enthalpy $\hat{h}$ and dynamic viscosity $\hat{\mu}$. The corresponding non-dimensional variables will be introduced similarly to (2.6):

$$\hat{u}' = \hat{V}_s u', \quad \hat{v}' = \hat{V}_s v', \quad \hat{p} = \hat{p}_s + \hat{\rho}_s \hat{V}_s^2 p,$$
$$\hat{\rho} = \hat{\rho}_s \rho, \quad \hat{h} = \hat{V}_s^2 h, \quad \hat{\mu} = \hat{\mu}_s \mu.$$
$$\hat{x} = Lx', \quad \hat{y} = Ly'.$$

Recall that suffix s is used to denote the values of the corresponding quantities on the free streamline as they are defined by the inviscid flow theory.

In the following analysis the Reynolds number

$$Re = \frac{\hat{\rho}_s \hat{V}_s L}{\hat{\mu}_s}$$

is assumed large, and the asymptotic expansions of the gas dynamic functions in the boundary layer are sought in the form

$$\left.\begin{aligned} u'(x', y'; Re) &= U_0(x', Y) + \cdots, \quad & v'(x', y'; Re) &= Re^{-1/2} V_0(x', Y) + \cdots, \\ p(x', y'; Re) &= P_0(x', Y) + \cdots, \quad & \rho(x', y'; Re) &= R_0(x', Y) + \cdots, \\ h(x', y'; Re) &= h_0(x', Y) + \cdots, \quad & \mu(x', y'; Re) &= \mu_0(x', Y) + \cdots, \end{aligned}\right\} \tag{3.1}$$

where, as usual, the coordinate normal to the wall is scaled as

$$y' = Re^{-1/2} Y.$$

Substitution of (3.1) into the Navier–Stokes equations gives the following set of equations:

$$R_0\left(U_0 \frac{\partial U_0}{\partial x'} + V_0 \frac{\partial U_0}{\partial Y}\right) = -\frac{\partial P_0}{\partial x'} + \frac{\partial}{\partial Y}\left(\mu_0 \frac{\partial U_0}{\partial Y}\right), \tag{3.2}$$

$$R_0\left(U_0 \frac{\partial h_0}{\partial x'} + V_0 \frac{\partial h_0}{\partial Y}\right) = U_0 \frac{\partial P_0}{\partial x'} + \frac{1}{Pr} \frac{\partial}{\partial Y}\left(\mu_0 \frac{\partial h_0}{\partial Y}\right) + \mu_0 \left(\frac{\partial U_0}{\partial Y}\right)^2, \tag{3.3}$$

$$\frac{\partial (R_0 U_0)}{\partial x'} + \frac{\partial (R_0 V_0)}{\partial Y} = 0, \tag{3.4}$$

$$h_0 = \frac{1}{(\gamma - 1) R_0} + \frac{\gamma}{\gamma - 1} \frac{P_0}{R_0}. \tag{3.5}$$

Equations (3.2)–(3.5) are in turn the momentum equation projected upon the longitudinal coordinate x', the energy equation with Pr being the Prandtl number, the continuity equation and the state equation.

To the leading order the pressure in the boundary layer does not change across the boundary layer

$$\frac{\partial P_0}{\partial Y} = 0,$$

which is easily confirmed by substituting (3.1) into the y'-component of the momentum

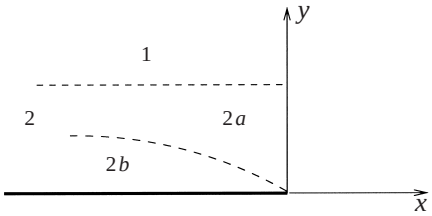

FIGURE 5. Boundary layer upstream of the interaction region.

equation. Hence, using (2.64), we have

$$\frac{\partial P_0}{\partial x'} = -\frac{N}{3(\gamma+1)}(-x')^{-2/3} + \cdots \quad \text{as} \quad x' \to 0^-. \tag{3.6}$$

3.1. *Region 2b*

The boundary layer, in the following discussion referred to as region 2, being exposed to the singular pressure gradient (3.6) splits up, as $x' \to 0^-$, into two subregions – the main part of the boundary layer shown as region 2*a* in figure 5 and the near-wall sublayer 2*b*.

We shall start our analysis with the sublayer. Taking into account that the fluid particles in region 2*b* experience extreme acceleration caused by the singular pressure gradient we expect that the convective terms on the left-hand side of the momentum equation (3.2) are of the same order of magnitude as the pressure gradient on the right-hand side. This may be expressed as

$$R_0 U_0 \frac{\partial U_0}{\partial x'} \sim \frac{\partial P_0}{\partial x'}. \tag{3.7}$$

Keeping in mind the no-slip condition at the aerofoil surface that has to be satisfied by the solution in region 2*b*, we further suppose that the flow in this region is viscous, i.e.

$$R_0 U_0 \frac{\partial U_0}{\partial x'} \sim \frac{\partial}{\partial Y}\left(\mu_0 \frac{\partial U_0}{\partial Y}\right). \tag{3.8}$$

We shall denote the value of the non-dimensional enthalpy h_0 at the 'bottom' of the boundary layer just upstream of the angular point O by h_w. The corresponding values of the non-dimensional density R_0 and viscosity μ_0 will be denoted as ρ_w and μ_w respectively. If the aerofoil is not artificially heated or cooled then ρ_w and μ_w are order-one quantities. Taking this into account we can deduce from (3.7) and (3.6) that in the viscous sublayer 2*b*

$$U_0 \sim (-x')^{1/6}. \tag{3.9}$$

Using (3.9) in (3.8) yields the following estimate for the thickness of region 2*b*:

$$Y \sim (-x')^{5/12}. \tag{3.10}$$

The second velocity component V_0 may be estimated using the continuity equation (3.4). Alternatively, we can introduce the stream function $\Psi_0(x', Y)$ such that

$$\frac{\partial \Psi_0}{\partial Y} = R_0 U_0, \quad \frac{\partial \Psi_0}{\partial x'} = -R_0 V_0. \tag{3.11}$$

As follows from the first of equations (3.11)

$$\Psi_0 \sim U_0 Y \sim (-x')^{7/12}.$$

Therefore the asymptotic expansion of the stream function in the viscous sublayer 2*b* should be sought in the form

$$\Psi_0(x', Y) = (-x')^{7/12}\psi(\eta) + \cdots \quad \text{as} \quad x' \to 0^-, \tag{3.12}$$

where, on account of (3.10), the independent variable

$$\eta = \frac{Y}{(-x')^{5/12}}. \tag{3.13}$$

To determine the form of the asymptotic expansions of the density R_0 and dynamic viscosity μ_0 one needs to estimate the temperature variations in region 2*b*. For this purpose the energy equation (3.3) should be used. Comparing the heat transfer term on the right-hand side of this equation with the mechanical energy dissipation

$$\frac{1}{Pr}\frac{\partial}{\partial Y}\left(\mu_0\frac{\partial h_0}{\partial Y}\right) \sim \mu_0\left(\frac{\partial U_0}{\partial Y}\right)^2$$

we see that the variations of the enthalpy

$$|h_0 - h_w| \sim U_0^2 \sim (-x')^{1/3}.$$

Now, using the state equation (3.5) we have

$$|R_0 - \rho_w| \sim (-x')^{1/3},$$

and, since the viscosity μ_0 is a function of the enthalpy,

$$|\mu_0 - \mu_w| \sim (-x')^{1/3}.$$

This shows that the asymptotic expansions of the density and viscosity sought in region 2*b* may be represented in the form

$$\left.\begin{aligned} R_0(x', Y) &= \rho_w + (-x')^{1/3}\tilde{\rho}(\eta) + \cdots \\ \mu_0(x', Y) &= \mu_w + (-x')^{1/3}\tilde{\mu}(\eta) + \cdots \end{aligned}\right\} \quad \text{as} \quad x' \to 0^-. \tag{3.14}$$

Substitution of (3.12), (3.13) and (3.14) into (3.11) and then into (3.2) results in the following equation for $\psi(\eta)$:

$$\mu_w\psi''' - \tfrac{7}{12}\psi\psi'' + \tfrac{1}{6}(\psi')^2 + \frac{N\rho_w}{3(\gamma+1)} = 0. \tag{3.15}$$

It should be solved with the no-slip condition on the aerofoil surface

$$\psi(0) = \psi'(0) = 0$$

and a condition that $\psi(\eta)$ does not grow exponentially at large values of η.† In this case the solution of (3.15) may be represented near the outer edge of the viscous sublayer by the asymptotic expansion

$$\psi(\eta) = A\eta^{7/5} + B\eta^{3/5} + C\eta^{2/5} + D\eta^{-1/5} + \cdots \quad \text{as} \quad \eta \to \infty, \tag{3.16}$$

where

$$B = -\frac{25}{7}\frac{N\rho_w}{A(\gamma+1)}, \quad D = \frac{5}{14}\frac{B^2}{A},$$

while the constants A and C remain arbitrary from the standpoint of a 'local' analysis

† Exponential growth of function $\psi(\eta)$ would make it impossible to match solutions in regions 2*b* and 2*a*.

of equation (3.15) at large values of η. However they may be found if a 'global' solution of (3.15) on the entire interval $\eta \in [0, \infty)$ is constructed, say, by means of numerical integration. Before performing the calculations it is convenient to apply the affine transformation

$$\psi = \mu_w^{1/2} N^{1/4} \rho_w^{1/4} (\gamma + 1)^{-1/4} \bar{\psi}, \quad \eta = \mu_w^{1/2} N^{-1/4} \rho_w^{-1/4} (\gamma + 1)^{1/4} \bar{\eta}$$

which reduces (3.15) to

$$\bar{\psi}''' - \tfrac{7}{12} \bar{\psi} \bar{\psi}'' + \tfrac{1}{6} (\bar{\psi}')^2 + \tfrac{1}{3} = 0. \tag{3.17}$$

Numerical solution of this equation was performed within a finite interval $\bar{\eta} \in [0, \bar{\eta}_{\max}]$, where $\bar{\eta}_{\max} = 20$ was typically taken. A uniform grid was used with either 1000 or 4000 node points. Control calculations were also performed with $\bar{\eta}_{\max} = 10$ to check the mesh independence of the results.

In order to avoid dealing with exponential growth of the solution as $\bar{\eta}$ becomes large, equation 3.17 was calculated starting from $\bar{\eta}_{\max}$ and progressing towards $\bar{\eta} = 0$. In this procedure the Runge–Kutta scheme was used. The values of $\bar{\psi}$ and the derivatives $\bar{\psi}'$, $\bar{\psi}''$ at $\bar{\eta} = \bar{\eta}_{\max}$ were calculated using formula (3.16) for which purpose it was rewritten in the transformed variables

$$\bar{\psi}(\bar{\eta}) = \bar{A} \bar{\eta}^{7/5} + \bar{B} \bar{\eta}^{3/5} + \bar{C} \bar{\eta}^{2/5} + \bar{D} \bar{\eta}^{-1/5} + \cdots \quad \text{as} \quad \bar{\eta} \to \infty.$$

Constants $\bar{A}$ and $\bar{C}$ in this formula are not known in advance and should be adjusted in such a way that the solution satisfies the no-slip conditions $\bar{\psi} = \bar{\psi}' = 0$ at $\bar{\eta} = 0$. The following iteration procedure, based on the Newtonian method, was employed to find appropriate values of $\bar{A}$, $\bar{C}$. Given that $\bar{A}$ and $\bar{C}$ are known from the previous iteration $\bar{A} = \bar{A}^i$, $\bar{C} = \bar{C}^i$, solution of equation (3.17) is constructed on the interval $[0, \bar{\eta}_{\max}]$ and, in particular, the values of $\bar{\psi}(0)$ and $\bar{\psi}'(0)$ are found. Then the calculations are repeated for $\bar{A} = \bar{A}^i + \Delta$, $\bar{C} = \bar{C}^i$, where the increment Δ of constant $\bar{A}$ should be chosen small enough, say, $\Delta = 0.01$. This yields slightly perturbed values of $\bar{\psi}(0)$ and $\bar{\psi}'(0)$. They can be used to calculate the derivatives of $\bar{\psi}(0)$ and $\bar{\psi}'(0)$ with respect to $\bar{A}$. To determine the derivatives of $\bar{\psi}(0)$ and $\bar{\psi}'(0)$ with respect to $\bar{C}$, equation (3.17) should be calculated for the third time, now with $\bar{A} = \bar{A}^i$, $\bar{C} = \bar{C}^i + \Delta$.

If we denote $\bar{\psi}(0)$ and $\bar{\psi}'(0)$ by M and N respectively, then according to Newton's method we can find the 'corrections' $\delta\bar{A}$, $\delta\bar{C}$ to $\bar{A}^i$ and $\bar{C}^i$ from the equations

$$M(\bar{A}^i + \delta\bar{A}, \bar{C}^i + \delta\bar{C}) = M(\bar{A}^i, \bar{C}^i) + \frac{\partial M}{\partial \bar{A}} \delta\bar{A} + \frac{\partial M}{\partial \bar{C}} \delta\bar{C} = 0,$$

$$N(\bar{A}^i + \delta\bar{A}, \bar{C}^i + \delta\bar{C}) = N(\bar{A}^i, \bar{C}^i) + \frac{\partial N}{\partial \bar{A}} \delta\bar{A} + \frac{\partial N}{\partial \bar{C}} \delta\bar{C} = 0.$$

Solving these equations for $\delta\bar{A}$ and $\delta\bar{C}$ one can update constants $\bar{A}$ and $\bar{C}$

$$\bar{A}^{i+1} = \bar{A}^i + \delta\bar{A}, \quad \bar{C}^{i+1} = \bar{C}^i + \delta\bar{C},$$

and proceed to the next iteration. Starting with initial values $\bar{A}^0 = \bar{C}^0 = 1$ the process converges to

$$\bar{A} = 1.4146, \quad \bar{C} = -0.1827.$$

It takes 12 iterations for tolerance 10^{-6} to be reached.

Function $\bar{\psi}(\eta)$ and its derivative $\bar{\psi}'(\eta)$ are shown in figure 6. To determine coeffi-

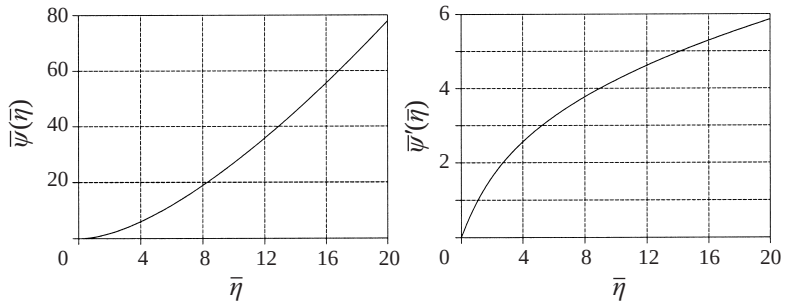

FIGURE 6. The results of the numerical solution of equation (3.15).

cients A and C of the asymptotic expansion (3.16) one has to use the formulae

$$A = \bar{A}\,\frac{N^{3/5}\rho_w^{3/5}}{\mu_w^{1/5}(\gamma+1)^{3/5}}, \quad C = \bar{C}\,\frac{N^{7/20}\rho_w^{7/20}\mu_w^{3/10}}{(\gamma+1)^{7/20}}.$$

3.2. *Region 2a*

With the purpose of finding the form of the solution in the main part of the boundary layer (region 2*a*) we substitute (3.16) into (3.12) and then into (3.11). This results in the expressions

$$\left.\begin{aligned} U_0 &= (-x')^{1/6}\left(\frac{7A}{5\rho_w}\eta^{2/5} + \frac{3B}{5\rho_w}\eta^{-2/5} + \cdots\right), \\ V_0 &= (-x')^{-5/12}\left(\frac{B}{3\rho_w}\eta^{3/5} + \frac{5C}{12\rho_w}\eta^{2/5} + \cdots\right), \end{aligned}\right\} \tag{3.18}$$

representing the velocity components at the outer edge of the viscous sublayer 2*b*. Using the principle of the matching of asymptotic expansions we can claim that the above formulae are valid in the overlap region situated between the viscous sublayer 2*b* and the main part of the boundary layer (region 2*a*). Therefore, they may be also used at the 'bottom' of region 2*a*. Rewriting (3.18) with the help of (3.13) we have

$$\left.\begin{aligned} U_0 &= \frac{7A}{5\rho_w}Y^{2/5} + \frac{3B}{5\rho_w}(-x')^{1/3}\frac{1}{Y^{2/5}} + \cdots, \\ V_0 &= \frac{B}{3\rho_w}(-x')^{-2/3}Y^{3/5} + \frac{5C}{12\rho_w}(-x')^{-7/12}Y^{2/5} + \cdots. \end{aligned}\right\} \tag{3.19}$$

This suggests that in region 2*a* where

$$Y = O(1), \quad x' \to 0^-,$$

asymptotic solution of the boundary-layer equations (3.2)–(3.5) should be sought in the form

$$\left.\begin{aligned} U_0(x', Y) &= U_{00}(Y) + (-x')^{1/3}U_{01}(Y) + \cdots, \\ V_0(x', Y) &= (-x')^{-2/3}V_{01}(Y) + \cdots, \\ R_0(x', Y) &= R_{00}(Y) + (-x')^{1/3}R_{01}(Y) + \cdots, \\ h_0(x', Y) &= h_{00}(Y) + (-x')^{1/3}h_{01}(Y) + \cdots, \\ \mu_0(x', Y) &= \mu_{00}(Y) + (-x')^{1/3}\mu_{01}(Y) + \cdots. \end{aligned}\right\} \tag{3.20}$$

It also follows from (3.19) that the matching conditions for the velocity components are

$$\left.\begin{aligned} U_{00}(Y) &= \frac{7A}{5\rho_w} Y^{2/5} + \cdots \\ V_{01}(Y) &= \frac{B}{3\rho_w} Y^{3/5} + \cdots \end{aligned}\right\} \quad \text{as} \quad Y \to 0. \tag{3.21}$$

Substitution of (3.20) into (3.2)–(3.5) results in the set of equations

$$-\tfrac{1}{3} R_{00} U_{00} U_{01} + R_{00} V_{01} U_{00}' = \frac{N}{3(\gamma+1)}, \tag{3.22}$$

$$-\tfrac{1}{3} R_{00} U_{00} h_{01} + R_{00} V_{01} h_{00}' = -\frac{N}{3(\gamma+1)} U_{00}, \tag{3.23}$$

$$\tfrac{1}{3} R_{00} U_{01} + \tfrac{1}{3} U_{00} R_{01} = R_{00} V_{01}' + R_{00}' V_{01}, \tag{3.24}$$

$$h_{00} = \frac{1}{(\gamma-1)R_{00}}, \quad h_{01} = -\frac{1}{\gamma-1}\frac{R_{01}}{R_{00}^2} + \frac{\gamma N}{\gamma^2-1}\frac{1}{R_{00}}. \tag{3.25}$$

Substituting (3.25) into the energy equation (3.23) and combining the result with the continuity equation (3.24) yields

$$V_{01}' - \tfrac{1}{3} U_{01} = \frac{N}{3(\gamma+1)} U_{00}. \tag{3.26}$$

Using (3.26) we can eliminate U_{01} from the momentum equation (3.22), which leads to

$$\frac{\mathrm{d}}{\mathrm{d}Y}\left(\frac{V_{01}}{U_{00}}\right) = \frac{N}{3(\gamma+1)}\left(1 - \frac{1}{R_{00}U_{00}^2}\right). \tag{3.27}$$

Note that despite U_{00} tending to zero as $Y \to 0$, the right-hand side in (3.27) is integrable, and since in accord with (3.21), $V_{01}/U_{00} = 0$ at $Y = 0$, we have

$$\frac{V_{01}}{U_{00}} = \frac{N}{3(\gamma+1)} \int_0^Y \left(1 - \frac{1}{M_{00}^2}\right) \mathrm{d}Y. \tag{3.28}$$

Here function $M_{00}(Y) = U_{00}\sqrt{R_{00}}$ gives the distribution of the Mach number across the boundary layer immediately upstream of the interaction region; the latter will be considered in the next section.

Before proceeding to the analysis of the interaction process let us consider the slope of the streamlines in region 2*a*. It may be measured by the angle θ made by the velocity vector with the aerofoil surface. Using (3.1), (3.20) and (3.28) we find that

$$\theta = \frac{v'}{u'} = Re^{-1/2}(-x')^{-2/3} \frac{N}{3(\gamma+1)} \int_0^Y \left(1 - \frac{1}{M_{00}^2}\right) \mathrm{d}Y. \tag{3.29}$$

For comparison, in viscous sublayer 2*b*, where the flow functions are represented by expansions (3.12), (3.11), the slope angle is estimated as

$$\theta \sim Re^{-1/2}(-x')^{-7/12}. \tag{3.30}$$

This shows that as $x' \to 0^-$ the displacement effect of the viscous sublayer becomes progressively smaller compared with the displacement effect of the main part of the boundary layer. Therefore, when analysing the interaction region the contribution of the sublayer can be neglected.

4. The interaction region

To find the slope of the streamlines at the outer edge of the boundary layer we let $Y \to \infty$ in (3.29). This yields

$$\theta = -Re^{-1/2}(-x')^{-2/3}\frac{N\mathscr{L}}{3(\gamma+1)}, \tag{4.1}$$

where

$$\mathscr{L} = \int_0^\infty \left(\frac{1}{M_{00}^2} - 1\right) \mathrm{d}Y$$

is referred to as Pearson's integral (see Pearson, Holliday & Smith 1958). Since $M_{00}(Y) \to 1$ as $Y \to \infty$, this integral is defined.

Now we can estimate the pressure perturbations p' induced in the flow by the displacement effect of the boundary layer. Recall that the derivation of § 2.2 serves to calculate the pressure field in the inviscid transonic flow past a thin aerofoil, the aerofoil surface slope being an $O(\delta)$ quantity and the pressure perturbation being $O(\delta^{2/3})$. Using θ as defined by (4.1) instead of δ we have

$$p' \sim \theta^{2/3} \sim Re^{-1/3}(-x')^{-4/9}.$$

We see that the pressure induced by the displacement effect of the boundary layer experiences unbounded growth as the separation point is approached, and despite the small coefficient $Re^{-1/3}$ it may become of the same order of magnitude as the pressure (2.64) exerted upon the boundary layer. This happens when

$$Re^{-1/3}(-x')^{-4/9} \sim (-x')^{1/3}. \tag{4.2}$$

Solving (4.2) for $(-x')$ gives the following estimate for the longitudinal extent of the interaction region:

$$|x'| = O(Re^{-3/7}). \tag{4.3}$$

In the vicinity of the separation point defined by (4.3) the pressure acting upon the boundary layer can no longer be treated as independent of the flow inside the boundary layer. The interaction region is shown graphically in figure 7. It has the usual triple-deck structure, being composed of the viscous sublayer (region 5), the main part of the boundary layer (region 4) and the external inviscid region 3 situated outside the boundary layer. The viscous sublayer is a continuation of region 2*b*, and unlike in many interactive flows studied before (a display of such studies may be found in Sychev *et al.* 1998), it is not expected to produce a noticeable contribution to the displacement effect of the boundary layer. Its role is merely to enforce the no-slip condition on the body surface upstream of the separation and to smooth out the velocity variation across the shear layer forming along the free streamline OS downstream of the separation. Region 4 represents a continuation of region 2*a*. Being exposed to a pressure gradient it is capable of generating a significantly larger slope of the streamlines compared with region 5. In region 3 the slope of the streamlines produced in region 4 is 'converted' into a perturbation of the pressure gradient which then acts back onto the flow in regions 4 and 5. Also shown in figure 7 is the inviscid region 1 which was studied in §§ 1 and 2.

To enable the theory of the interaction to describe the influence of the Mach number on the flow behaviour in the interaction region we shall choose parameter ϵ in (2.15) to be

$$\epsilon = Re^{-1/7}, \tag{4.4}$$

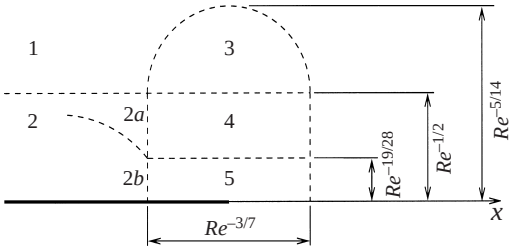

FIGURE 7. A sketch of the interaction region.

in which case the estimates (2.79) and (4.3) coincide with each other.

For investigating the flow in the interaction region it is convenient to return to the Cartesian coordinate system introduced in § 2. We shall start with the main part of the boundary layer, region 4.

4.1. *Region 4*

Asymptotic analysis of the Navier–Stokes equations in region 4 is based on the limit procedure

$$x_* = Re^{3/7}x' = O(1), \quad Y = O(1), \quad Re \to \infty.$$

Gas dynamic functions may be represented in this region by the asymptotic expansions

$$\left.\begin{aligned} u'(x,y;Re) &= U_{00}(Y) + Re^{-1/7}\tilde{U}_1(x_*,Y) + \cdots, \\ v'(x,y;Re) &= Re^{-3/14}\tilde{V}_1(x_*,Y) + \cdots, \\ p(x,y;Re) &= Re^{-1/7}\tilde{P}_1(x_*,Y) + \cdots, \\ \rho(x,y;Re) &= R_{00}(Y) + Re^{-1/7}\tilde{R}_1(x_*,Y) + \cdots, \\ h(x,y;Re) &= h_{00}(Y) + Re^{-1/7}\tilde{h}_1(x_*,Y) + \cdots, \\ \mu(x,y;Re) &= \mu_{00}(Y) + Re^{-1/7}\tilde{\mu}_1(x_*,Y) + \cdots, \end{aligned}\right\} \tag{4.5}$$

the form of which is easily predicted by expressing the solution (3.1), (3.20), (2.64) in region 2*a* via the variables x_*, Y of region 4.

Substitution of (4.5) together with (2.15) and (4.4) into the Navier–Stokes equations reduces the longitudinal momentum equation to

$$R_{00}U_{00}\frac{\partial\tilde{U}_1}{\partial x_*} + R_{00}\tilde{V}_1U'_{00} = -\frac{\partial\tilde{P}_1}{\partial x_*}. \tag{4.6}$$

The energy equation becomes

$$R_{00}U_{00}\frac{\partial\tilde{h}_1}{\partial x_*} + R_{00}\tilde{V}_1h'_{00} = U_{00}\frac{\partial\tilde{P}_1}{\partial x_*}. \tag{4.7}$$

The continuity equation may be written as

$$R_{00}\frac{\partial\tilde{U}_1}{\partial x_*} + U_{00}\frac{\partial\tilde{R}_1}{\partial x_*} + R_{00}\frac{\partial\tilde{V}_1}{\partial Y} + \tilde{V}_1R'_{00} = 0, \tag{4.8}$$

and the two-term approximation of the state equation yields

$$h_{00} = \frac{1}{(\gamma-1)R_{00}}, \quad \tilde{h}_1 = -\frac{1}{\gamma-1}\left(\frac{\tilde{R}_1}{R_{00}^2} + \frac{2M_1}{R_{00}}\right) + \frac{\gamma}{\gamma-1}\frac{\tilde{P}_1}{R_{00}}. \tag{4.9}$$

It also follows from the momentum equation projected onto the y-axis that

$$\frac{\partial \tilde{P}_1}{\partial Y} = 0,$$

hence the pressure $\tilde{P}_1$ appears to be a function of x_* only.

Equations (4.6)–(4.9) may be dealt with in the same way as equations (3.22)–(3.25). Substituting (4.9) into the energy equation (4.7) and combining the result with the continuity equation (4.8) we find

$$\frac{\partial \tilde{U}_1}{\partial x_*} = -\frac{\partial \tilde{V}_1}{\partial Y} - U_{00}\frac{\mathrm{d}\tilde{P}_1}{\mathrm{d}x_*}. \tag{4.10}$$

Substitution of (4.10) into the momentum equation (4.6) yields the following expression for the slope of the streamlines in region 4:

$$\frac{\tilde{V}_1}{U_{00}} = \frac{\mathrm{d}\tilde{P}_1}{\mathrm{d}x_*}\int_0^Y \left(\frac{1}{M_{00}^2} - 1\right)\mathrm{d}Y.$$

In particular, at the outer edge of region 4

$$\frac{\tilde{V}_1}{U_{00}} = \mathscr{L}\frac{\mathrm{d}\tilde{P}_1}{\mathrm{d}x_*} + \cdots \quad \text{as} \quad Y \to \infty, \tag{4.11}$$

where $\mathscr{L}$ is Pearson's integral.

We shall now study the response of the flow in region 3 to the displacement effect of region 4.

4.2. *Region 3*

Asymptotic analysis of the Navier–Stokes equations in region 3 is based on the limit procedure

$$x_* = Re^{3/7}x = O(1), \quad y_* = Re^{5/14}y = O(1), \quad Re \to \infty. \tag{4.12}$$

Note that in the interaction region the curvilinear coordinates x', y' are indistinguishable from Cartesian coordinates x, y introduced in § 2, and x_* is common for regions 3 and 4; the scaling of the y-coordinate has been determined by substituting (4.4) into (2.78). It could also have been determined by recognizing that ξ, as defined by (2.25), remains an order-one quantity when 'entering' the upper layer (region 3) of the interaction region. The flow in this layer is expected to be described again by the Kármán–Guderley equation of the form (2.44).

In order to find the form of the solution in region 3 one can use expansion (2.77). Being rewritten in terms of the variables (4.12) it becomes

$$\Phi = Re^{-3/7}x_* + Re^{-4/7}\frac{1}{\gamma+1}\left[y_*^{8/5}F_0(\xi) + y_*^{6/5}F_1(\xi)\right] + \cdots,$$

which suggests that the potential Φ should be sought in region 3 in the form of the asymptotic expansion

$$\Phi(x, y; Re) = Re^{-3/7}x_* + Re^{-4/7}\Phi_1^*(x_*, y_*) + \cdots \quad \text{as} \quad Re \to \infty. \tag{4.13}$$

The analysis of the flow in region 3 may be performed based on either the Navier–Stokes equations or, equivalently, on the inviscid equations (2.7)–(2.11). Substitution of (4.13) into (2.8) shows that asymptotic expansions of the velocity components are

$$\left.\begin{aligned} u(x, y; Re) &= 1 + Re^{-1/7}u_1^*(x_*, y_*) + \cdots, \\ v(x, y; Re) &= Re^{-3/14}v_1^*(x_*, y_*) + \cdots, \end{aligned}\right\} \tag{4.14}$$

where

$$u_1^* = \frac{\partial \Phi_1^*}{\partial x_*}, \quad v_1^* = \frac{\partial \Phi_1^*}{\partial y_*}. \tag{4.15}$$

Using (4.14) in equation (2.9), with M_s defined by (2.15) and (4.4), it may be easily found that the speed of sound

$$a(x, y; Re) = 1 + Re^{-1/7} a_1^*(x_*, y_*) + \cdots, \tag{4.16}$$

and

$$a_1^* = -\frac{\gamma - 1}{2} u_1^* - M_1. \tag{4.17}$$

Similarly, from (2.10), (2.11) it follows that the pressure

$$p(x, y; Re) = Re^{-1/7} p_1^*(x_*, y_*) + \cdots,$$

with p_1^* being related to the longitudinal velocity component u_1^* as

$$p_1^* = -u_1^*. \tag{4.18}$$

Substitution of (4.14), (4.16) and (4.17) into (2.7) leads to the first equation relating u_1^* and v_1^*:

$$\left[2M_1 + (\gamma + 1)u_1^*\right] \frac{\partial u_1^*}{\partial x_*} - \frac{\partial v_1^*}{\partial y_*} = 0. \tag{4.19}$$

The second one may be derived by cross-differentiation of (4.15):

$$\frac{\partial u_1^*}{\partial y_*} - \frac{\partial v_1^*}{\partial x_*} = 0. \tag{4.20}$$

Boundary conditions for these equations may be formulated (i) by matching the slope of the streamlines v/u in regions 3 and 4 which, in view of (4.11) and (4.18), leads to

$$v_1^* = -\mathscr{L} \frac{\partial u_1^*}{\partial x_*} \quad \text{at} \quad y_* = 0, \quad x_* < 0, \tag{4.21}$$

(ii) by imposing a condition that pressure (4.18) remains constant along the free streamline

$$u_1^* = 0 \quad \text{at} \quad y_* = 0, \quad x_* > 0, \tag{4.22}$$

and (iii) by matching the velocity components in regions 3 and 1. The leading-order solution in region 1 is expressed implicitly by equations (2.61), (2.62). Using (2.42) and (2.47), these may be rewritten as

$$\tilde{y} = \frac{C}{\delta^{5/3}} (\gamma + 1)^2 (u_0 - 1) v_0,$$

$$x = \frac{C(\gamma + 1)^3}{3\delta^2} (u_0 - 1)^3 + \frac{C(\gamma + 1)^2}{2\delta^2} v_0^2.$$

Taking into account that $C = 3\delta^2/N^3$ and $\tilde{y} = \delta^{1/3} y$ we can express these equations as

$$\left.\begin{aligned} y &= \frac{3}{N^3} (\gamma + 1)^2 (u - 1) v, \\ x &= \frac{(\gamma + 1)^3}{N^3} (u - 1)^3 + \frac{3}{2} \frac{(\gamma + 1)^2}{N^3} v^2. \end{aligned}\right\} \tag{4.23}$$

It remains to substitute (4.12) and (4.14) into (4.23) and we will have the boundary

condition sought in the form

$$\left.\begin{aligned} y_* &= \frac{3}{N^3}(\gamma+1)^2 u_1^* v_1^*, \\ x_* &= \frac{(\gamma+1)^3}{N^3} u_1^{*3} + \frac{3}{2}\frac{(\gamma+1)^2}{N^3} v_1^{*2} \end{aligned}\right\} \quad \text{as} \quad x_*^2 + y_*^2 \to \infty. \tag{4.24}$$

Formulae (4.24) remain uniformly valid for all $x_*/y_*^{6/5} \in (-\infty, \infty)$.

Equations (4.19), (4.20) considered with boundary conditions (4.21), (4.22) and (4.24) constitute the interaction problem. They may be more conveniently written by performing the following affine transformations:

$$\begin{aligned} u_1^* &= \frac{1}{\gamma+1}\mathscr{L}^{2/7} N^{6/7} u, \qquad v_1^* = \frac{1}{\gamma+1}\mathscr{L}^{3/7} N^{9/7} v, \\ x_* &= \mathscr{L}^{6/7} N^{-3/7} x, \qquad\qquad y_* = \mathscr{L}^{5/7} N^{-6/7} y. \end{aligned}$$

As a result the equations describing the flow take the form

$$(\mathscr{K} - u)\frac{\partial u}{\partial x} + \frac{\partial v}{\partial y} = 0, \quad \frac{\partial u}{\partial y} - \frac{\partial v}{\partial x} = 0. \tag{4.25}$$

These have to be solved with the boundary conditions

$$\left.\begin{aligned} v &= -\frac{\partial u}{\partial x}, \quad x < 0 \\ u &= 0, \qquad\quad x > 0 \end{aligned}\right\} \quad \text{at} \quad y = 0, \tag{4.26}$$

and

$$\left.\begin{aligned} y &= 3uv, \\ x &= u^3 + \tfrac{3}{2}v^2 \end{aligned}\right\} \quad \text{as} \quad x^2 + y^2 \to \infty. \tag{4.27}$$

The similarity parameter in (4.25) is defined as

$$\mathscr{K} = -\frac{2M_1}{\mathscr{L}^{2/7} N^{6/7}}.$$

It has the same physical meaning as the Kármán–Guderley parameter. It is positive when the velocity on the separation stream line is 'slightly subsonic' and negative when this velocity is 'slightly supersonic'.

4.3. *Region 5*

Once the interaction problem (4.25)–(4.27) is solved and the distribution of pressure is found using Bernoulli's equation (4.18), one can proceed to the flow analysis in the viscous near-wall region 5 (see figure 7). This region represents a continuation of the viscous sublayer 2*b* into the interaction region. The form of the solution in region 5

$$\left.\begin{aligned} u' &= Re^{-1/14} U_*(x_*, Y_*) + \cdots, \quad v' = Re^{-9/28} V_*(x_*, Y_*) + \cdots, \\ p &= Re^{-1/7} P_*(x_*, Y_*) + \cdots, \quad \rho = \rho_w + \cdots, \quad \mu = \mu_w + \cdots, \\ x' &= Re^{-3/7} x_*, \quad y' = Re^{-19/28} Y_* \end{aligned}\right\} \tag{4.28}$$

may be therefore predicted by re-expanding solution (3.1), (3.11)–(3.13) and (3.14) in region 2*b* in terms of variables x_* and Y_* of region 5.

Substitution of 4.28 into the Navier–Stokes equations results in the incompressible

form of Prandtl's boundary-layer equations

$$\left.\begin{aligned} \rho_w\left(U_*\frac{\partial U_*}{\partial x_*}+V_*\frac{\partial U_*}{\partial Y_*}\right)&=-\frac{\mathrm{d}P_*}{\mathrm{d}x_*}+\mu_w\frac{\partial^2 U_*}{\partial Y_*^2},\\ \frac{\partial U_*}{\partial x_*}+\frac{\partial V_*}{\partial Y_*}&=0. \end{aligned}\right\} \tag{4.29}$$

They should be solved with the no-slip condition on the aerofoil surface

$$U_*=V_*=0 \quad \text{at} \quad Y_*=0, \quad x_*<0, \tag{4.30}$$

and conditions of matching with the solution (4.5), (3.21) in region 4

$$U_*=\frac{7A}{5\rho_w}Y_*^{2/5}+\cdots \quad \text{as} \quad Y_*\to\infty \tag{4.31}$$

and solution (3.1), (3.11)–(3.13) in region 2*b*

$$U_*=\frac{1}{\rho_w}(-x_*)^{1/6}\psi'(\eta)+\cdots \quad \text{as} \quad x_*\to-\infty. \tag{4.32}$$

In this last formula the similarity variable

$$\eta=\frac{Y_*}{(-x_*)^{5/12}}$$

is supposed to remain an order-one quantity as $x_*\to-\infty$.

Affine transformations

$$U_*=\frac{\mathscr{L}^{1/7}N^{3/7}}{(\gamma+1)^{1/2}\rho_w^{1/2}}U, \quad V_*=\frac{\mu_w^{1/2}N^{3/7}}{(\gamma+1)^{1/4}\rho_w^{3/4}\mathscr{L}^{5/14}}V, \quad P_*=\frac{\mathscr{L}^{2/7}N^{6/7}}{\gamma+1}P,$$

$$x_*=\mathscr{L}^{6/7}N^{-3/7}x, \quad Y_*=\frac{(\gamma+1)^{1/4}\mu_w^{1/2}\mathscr{L}^{5/14}}{\rho_w^{1/4}N^{3/7}}Y$$

allow the boundary-value problem (4.29)–(4.32) to be represented in the following form:

$$\left.\begin{aligned} U\frac{\partial U}{\partial x}+V\frac{\partial U}{\partial Y}&=-\frac{\mathrm{d}P}{\mathrm{d}x}+\frac{\partial^2 U}{\partial Y^2},\\ \frac{\partial U}{\partial x}+\frac{\partial V}{\partial Y}&=0,\\ U=V&=0 \quad \text{at} \quad Y=0, \quad x<0,\\ U&=\tfrac{7}{5}\bar{A}Y^{2/5}+\cdots \quad \text{as} \quad Y\to\infty,\\ U&=(-x)^{1/6}\bar{\psi}'(\bar{\eta})+\cdots \quad \text{as} \quad x\to-\infty. \end{aligned}\right\} \tag{4.33}$$

Here function $\bar{\psi}(\bar{\eta})$ is defined by equation (3.17); its argument $\bar{\eta}$ may be calculated via the transformed variables x, Y:

$$\bar{\eta}=\frac{Y}{(-x)^{5/12}}.$$

The pressure P does not vary across region 5 and is dictated by the solution of the interaction problem (4.25)–(4.27). In view of Bernoulli's equation (4.18) it can be calculated as

$$P=-u|_{y=0}.$$

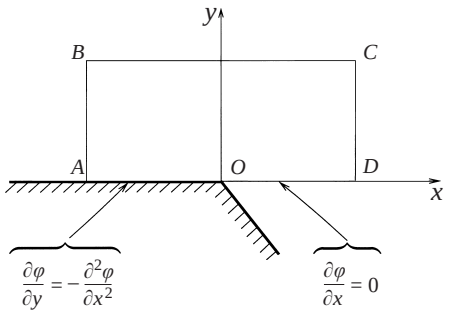

FIGURE 8. Computational domain.

5. Numerical solution of the interaction problem

For the purpose of numerical solution of the interaction problem it is convenient to write equations (4.25) in the form of the Kármán–Guderley equation

$$(\mathcal{K} - u)\frac{\partial^2\varphi}{\partial x^2} + \frac{\partial^2\varphi}{\partial y^2} = 0, \tag{5.1}$$

with the potential φ being related to the velocity components via

$$u = \frac{\partial\varphi}{\partial x}, \quad v = \frac{\partial\varphi}{\partial y}. \tag{5.2}$$

The calculations were performed in a rectangular domain $ABCD$ shown in figure 8. A uniform grid was adopted in both x- and y-directions. With (x_i, y_j) being the node points, the grid function for the potential φ was introduced according to the rule

$$\varphi_{i,j} = \varphi(x_i, y_j), \quad \text{for all} \begin{cases} i = 1, \ldots, I_0, \ldots, I_m, \\ j = 1, \ldots, J_m, \end{cases}$$

where $i = I_0$ corresponds to the angular point O.

To start the calculations one needs to specify the distribution of φ along the upstream, top and downstream boundaries of the computational domain. For this purpose equations (4.27) have to be used. At the point A where $y = 0$ the solution of (4.27) obviously is

$$u = -(-x_A)^{1/3}, \quad v = 0. \tag{5.3}$$

Differentiation of (4.27) with respect to y leads to the equations

$$\frac{\partial u}{\partial y} = \frac{v}{3(v^2 - u^3)}, \quad \frac{\partial v}{\partial y} = \frac{u^2}{3(u^3 - v^2)}, \tag{5.4}$$

which are easily integrated along the upstream boundary AB using (5.3) as the initial conditions. Once v is found, the second of equations (5.2) may be integrated to find the distribution of φ along AB. Since equations (5.2) define the potential φ to within an arbitrary constant, one can choose, for example, $\varphi = 0$ at the point A.

Differentiation of (4.27) with respect to x leads to the equations

$$\frac{\partial u}{\partial x} = \frac{u}{3(u^3 - v^2)}, \quad \frac{\partial v}{\partial x} = \frac{v}{3(v^2 - u^3)}.$$

They may be integrated along with the first of equations (5.2) to find the distribution of φ at the top boundary BC. Then equations (5.4) should be used again to calculate φ

at the downstream boundary CD. The accuracy of these calculations may be verified by comparing the numerical solution at the point D with the exact solution

$$v = -\sqrt{\tfrac{2}{3}\, x_D},$$

which is easily derived from the second of equations (4.27) by setting $u = 0$.

The solution inside the computational domain and along the bottom boundary AD was calculated by means of successive iterations. Each iteration consisted of two steps. First, the distribution of the potential φ was updated at all the internal points of the domain $ABCD$, and then φ was recalculated at the bottom boundary AD. The former procedure was based on the conventional line relaxation. Starting with the second mesh line ($i = 2$) we marched downstream through the computational domain to the last but one line ($i = I_m - 1$), and on each of the lines ($i = 2, \ldots, I_m - 1$) a tri-diagonal set of algebraic equations

$$a_j \varphi_{i,j+1} + b_j \varphi_{i,j} + c_j \varphi_{i,j-1} + d_j = 0, \quad j = 2, \ldots, J_{m-1}, \tag{5.5}$$

was formulated by the finite-difference approximation of the Kármán–Guderley equation (5.1). This is a mixed elliptic-hyperbolic equation, and a choice of the computational stencil at each grid point was based on the sign of $\mathscr{K} - u_{i,j}$; to calculate $u_{i,j}$ central-difference approximation of the first of equations (5.2) was used. If $\mathscr{K} - u_{i,j} \geqslant 0$ then equation (5.1) is 'locally' elliptic and should be approximated using central differences for both second-order derivatives of φ, i.e.

$$(\mathscr{K} - u_{i,j}) \frac{\varphi_{i+1,j} - 2\varphi_{i,j} + \varphi_{i-1,j}}{(\Delta x)^2} + \frac{\varphi_{i,j+1} - 2\varphi_{i,j} + \varphi_{i,j-1}}{(\Delta y)^2} = 0. \tag{5.6}$$

If on the other hand $\mathscr{K} - u_{i,j} < 0$, then a hyperbolic stencil with upstream differencing for $\partial^2 \varphi / \partial x^2$ should be used. In our calculations the following second-order-accurate approximation was adopted:

$$(\mathscr{K} - u_{i,j}) \frac{2\varphi_{i,j} - 5\varphi_{i-1,j} + 4\varphi_{i-2,j} - \varphi_{i-3,j}}{(\Delta x)^2} + \frac{\varphi_{i,j+1} - 2\varphi_{i,j} + \varphi_{i,j-1}}{(\Delta y)^2} = 0. \tag{5.7}$$

It follows from (5.6) and (5.7) that the coefficients in (5.5) may be calculated as

$$a_j = \frac{1}{(\Delta y)^2}, \quad b_j = -\frac{2}{(\Delta y)^2} - \frac{2}{(\Delta x)^2} |\mathscr{K} - u_{i,j}|, \quad c_j = \frac{1}{(\Delta y)^2},$$

$$d_j = \begin{cases} \dfrac{|\mathscr{K} - u_{i,j}|}{(\Delta x)^2} (\varphi_{i+1,j} + \varphi_{i-1,j}) & \text{if} \quad \mathscr{K} - u_{i,j} \geqslant 0, \\ \dfrac{|\mathscr{K} - u_{i,j}|}{(\Delta x)^2} (5\varphi_{i-1,j} - 4\varphi_{i-2,j} + \varphi_{i-3,j}) & \text{if} \quad \mathscr{K} - u_{i,j} < 0. \end{cases}$$

Note that $\varphi_{i-1,j}$, $\varphi_{i-2,j}$ and $\varphi_{i-3,j}$ have already been updated, while $\varphi_{i+1,j}$ should be taken from the previous iteration.

Two boundary conditions are required to solve equations (5.5). At the top boundary the value of φ_{i,J_m} given by the boundary condition (4.27) was used. At the bottom boundary $\varphi_{i,1}$ was taken from the previous iteration. The Thomas technique proved to be an efficient tool for solving (5.5) on each mesh line $x = x_i$.

After the marching through the computational domain was completed, the distribution of φ along the bottom boundary AD was updated using the following procedure. Upstream of the separation point the first of equations (4.26) is applicable. When

combined with (5.2) it takes the form

$$\frac{\partial \varphi}{\partial y} = -\frac{\partial^2 \varphi}{\partial x^2} \quad \text{at} \quad y = 0, \quad x < 0,$$

which may be written in finite differences as

$$\frac{4\varphi_{i,2} - 3\varphi_{i,1} - \varphi_{i,3}}{2\Delta y} = -\frac{\varphi_{i+1,1} - 2\varphi_{i,1} + \varphi_{i-1,1}}{(\Delta x)^2}, \quad i = 2, \ldots, I_0 - 1.$$

This leads to the following tri-diagonal set of equations:

$$a_i \varphi_{i+1,1} + b_i \varphi_{i,1} + c_i \varphi_{i-1,1} + d_i = 0, \quad i = 2, \ldots, I_0 - 1, \tag{5.8}$$

where

$$a_i = c_i = \frac{1}{(\Delta x)^2}, \quad b_i = -\frac{2}{(\Delta x)^2} - \frac{3}{2\Delta y}, \quad d_i = \frac{4\varphi_{i,2} - \varphi_{i,3}}{2\Delta y}.$$

Again two boundary conditions are needed. The first one follows from the convention that at the point A

$$\varphi_{1,1} = 0. \tag{5.9}$$

The second boundary condition is

$$u = \frac{\partial \varphi}{\partial x} = 0 \quad \text{at} \quad x = 0, \quad y = 0, \tag{5.10}$$

which implies that the pressure cannot have a discontinuity at the separation point. Using the second-order-accurate finite-difference approximation of (5.10) we have

$$3\varphi_{I_0,1} - 4\varphi_{I_0-1,1} + \varphi_{I_0-2,1} = 0. \tag{5.11}$$

To solve equations (5.8), (5.9), (5.11) the Thomas technique was used.

Finally, the distribution of φ along the free streamline was updated using the second of equations (4.26) from which it follows that

$$\varphi_{i,1} = \varphi_{I_0,1} \quad \text{for all} \quad i = I_0 + 1, \ldots, I_m - 1.$$

This two-step procedure was repeated as many times as required for the convergence criterion

$$\max_{i,j} \left| \varphi_{i,j}^{new} - \varphi_{i,j}^{old} \right| < \epsilon$$

to be met. Most calculations were performed with $\epsilon = 10^{-6}$; however a number of check cases were run with $\epsilon = 10^{-7}$. The size of the computational domain was first taken to be $x \in [-10, 10]$, $y \in [0, 10]$ and then the calculations were repeated on a larger domain with $x \in [-20, 20]$, $y \in [0, 20]$. The number of grid points was also varied from 150×75 to 500×250, and it is believed that the numerical results are accurate to within four digits.

Figure 9 shows the behaviour of pressure $p = -u$ along the aerofoil surface for different values of the Kármán–Guderley parameter. It is interesting that $p(x, 0)$ monotonically decreases with x, which means that the viscous flow in region 5 (see figure 7) is driven towards the separation point by a favourable pressure gradient. Under these conditions the solution of boundary-value problem 4.33 for region 5 exists by Theorem 2.1.1 in Oleinik & Samohin (1997). This theorem also guarantees that no separation can occur upstream of the corner point O.

Thus the strategy suggested earlier by Diesperov (1981, 1983) cannot be used to describe the transonic flow separation from an angular point. Diesperov surmised

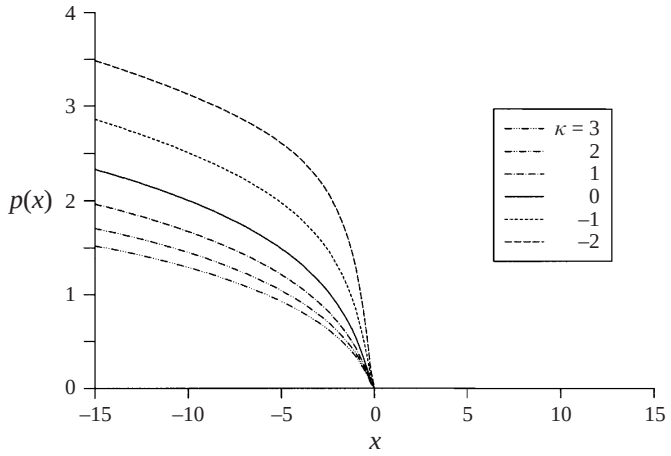

FIGURE 9. Pressure distribution in the interaction region for different values of the similarity parameter $\mathscr{K}$.

that a solution in region 5 could only exist if the pressure distribution along the boundary layer is properly adjusted. In other words, he expected that by solving Prandtl's equations in region 5 it would be possible to find not only the velocity field in the sublayer but also the pressure distribution along the body surface. He further argued that the flow in the external region 3 (see figure 7) could then be determined as follows. Using Bernoulli's equation $u = -p$ and the pressure distribution known from the solution in region 5, one would be able to calculate the distribution of v at the bottom of region 3. This may be done with the help of the first of equations (4.26). The velocity field in region 3 could then be determined by solving equations (4.25) with the known distribution of v at the bottom of region 3.

Diesperov's concept not only contradicts the flow analysis presented in this paper. It is also intrinsically inconsistent, and could not be implemented for the following reasons. First, Prandtl's boundary-layer equations, as has already been mentioned, do not allow determination of the distribution of pressure. Secondly, once equations (4.25) are solved, the pressure distribution in region 3 may be easily determined, and it should coincide with the pressure used initially to calculate the distribution of v at the bottom of region 3. Such a coincidence is not likely to happen.

6. Concluding remarks

It has been shown in this study that the boundary-layer separation from an angular point of a rigid body surface in transonic flow is accompanied by strong interaction between the external potential part of the flow and the boundary layer. This interaction governs the flow behaviour in the vicinity of the separation point with the longitudinal extent $x = O(Re^{-3/7})$. The interaction region has the usual triple-deck structure encountered in many other high Reynolds number flows studied earlier, including the incompressible flow separating from a convex corner of a rigid body surface. Analysis of this problem was performed by Ackerberg (1970, 1971) and Ruban (1974) (see also Sychev *et al.* 1998). They discovered that in incompressible flow the boundary layer approaching the separation point is exposed to the 'extremely

favourable' pressure gradient

$$\frac{\partial P_0}{\partial x'} = -\frac{K}{(-x')^{1/2}} + \cdots \quad \text{as} \quad x' \to 0^-,$$

where K is a positive constant. It causes a sharp acceleration of fluid particles in the boundary layer. As a result the velocity profile $U_{00}(Y)$ in the boundary layer immediately upstream of the interaction region appears to be such that

$$U_{00}(Y) = \tfrac{5}{3} A\, Y^{2/3} + \cdots \quad \text{as} \quad Y \to 0, \tag{6.1}$$

where $A = (2K^2)^{1/3} A_0$ with $A_0 = 1.9507$.

In the transonic flow the pressure gradient (3.6) is even more severe

$$\frac{\partial P_0}{\partial x'} = -\frac{N}{3(\gamma+1)}(-x')^{-2/3} + \cdots \quad \text{as} \quad x' \to 0^-.$$

It makes the velocity profile in the boundary layer behave according to the first formula in (3.21), i.e.

$$U_{00}(Y) = \frac{7A}{5\rho_w} Y^{2/5} + \cdots \quad \text{as} \quad Y \to 0. \tag{6.2}$$

To explain why there is a significant difference in the way the interaction process proceeds in these two flows, an analysis is performed in Appendix B under the assumption that

$$U_{00}(Y) = A Y^{1/m} + \cdots \quad \text{as} \quad Y \to 0, \tag{6.3}$$

with m being a positive constant, and it is shown that the contribution of the sublayer to the displacement effect of the boundary layer is comparable with that of the main part of the boundary layer provided that $m = 2$. In most boundary-layer flows the longitudinal velocity U_{00} grows linearly with Y near the bottom of the boundary layer:

$$U_{00}(Y) = \tau_w Y + \cdots \quad \text{as} \quad Y \to 0, \tag{6.4}$$

which corresponds to $m = 1$. This explains why the sublayer displacement effect is normally dominant. To the same category belongs the incompressible flow separating from a convex corner. In this case formula (6.1) is valid, giving $m = 3/2$ which is still less than the critical value $m = 2$. However, in the transonic flow studied in this paper $m = 5/2$, as may be easily seen from (6.2), and it is not surprising that interaction takes place between the external flow and the main part of the boundary layer. It therefore may be referred to as *inviscid–inviscid interaction.*

Comparing (3.29) with (3.30) one can conclude that in the interaction region where $x' \sim O(Re^{-3/7})$ the relative error arising from neglecting the displacement effect of the viscous sublayer is $O(Re^{-1/28})$, not really very small. This suggests that increasing the Mach number perturbation ϵ compared to (4.4) should soon lead to a new asymptotic regime in which the contributions of both the main part of the boundary layer and the viscous sublayer have to be taken into account in the leading-order approximation.

There is an apparent analogy with hypersonic boundary-layer separation from a cold wall. While in the boundary layer developing along a cold body surface the velocity profile still behaves linearly (5.4) near the wall, the non-dimensional skin friction τ_w can no longer be considered an order-one quantity. In fact, the smaller the wall temperature the larger τ_w appears to be. Hence the effect of the wall cooling is similar to increasing m in (5.3). Keeping this in mind Neiland (1973) demonstrated that the main part of the boundary layer starts to play a significant role in the

interaction process when the wall temperature is reduced to a certain level. Later, different aspects of the theory of hypersonic boundary-layer separation on a cold wall including flow regimes with inviscid–inviscid interaction were studied by Neiland & Sokolov (1975), Brown, Cheng & Lee (1990), Messiter, Matarrese & Adamson (1991) and Kerimbekov, Ruban & Walker (1994).

For a different reason, the main part of the boundary layer plays a major role in still another interaction regime (see Messiter & Liñáñ 1976; Shidlovskii 1977; Smith & Duck 1977) taking place, for example, when viscous near-wall jet separates from a solid body surface. In this case the velocity is zero in the external flow, and the pressure is constant at the outer edge of the boundary layer. The pressure perturbations inside the boundary layer are produced by the centrifugal effect coming into action as a result the curving of the streamlines in the boundary layer. If in the main part of the boundary layer the streamlines are distorted by the displacement effect of the viscous sublayer, then the pressure starts to change across the boundary layer. As a result the viscous sublayer is under the action of the induced pressure gradient which supports the displacement effect of the sublayer and the entire interaction process.

Appendix A

The analysis in § 2 is based on the assumption that the flow at hand is irrotational. We shall now present a justification of this assumption, for which purpose Crocco's formula

$$\boldsymbol{V} \times \boldsymbol{\omega} = -T\nabla S \tag{A 1}$$

and entropy conservation law

$$\boldsymbol{V} \cdot \nabla S = 0 \tag{A 2}$$

will be used. The expression on the left-hand side of the Crocco's formula is the vector product of the velocity vector $\boldsymbol{V}$ and vorticity $\boldsymbol{\omega} = \nabla \times \boldsymbol{V}$. Function T on the right-hand side represents the gas temperature, and ∇S is the gradient of the entropy.

Equations (A 1) and (A 2) hold in any inviscid gas flow. From (A 2) it follows that the entropy S stays constant along the streamlines. Therefore, if the flow is free of shock waves and all the streamlines (in the part of the flow of interest) 'originate' from the uniform flow upstream of the aerofoil, then $S = S_\infty$ and Crocco's formula (A 1) reduces to

$$\boldsymbol{V} \times \boldsymbol{\omega} = 0. \tag{A 3}$$

In two-dimensional flows the vorticity $\boldsymbol{\omega}$ is always perpendicular to the velocity vector $\boldsymbol{V}$. Hence, everywhere except perhaps at the stagnation point, one has to set $\boldsymbol{\omega} = 0$ to satisfy equation (A 3).

Suppose now that a shock wave forms in the flow. Then, in accordance with (A 2), the entropy S remains constant along a streamline upstream and downstream of the shock. However, when the streamline crosses the shock the entropy increases by an amount ΔS which in general is different for different streamlines. Therefore the entropy S is no longer constant downstream of the shock and, strictly speaking, the vorticity cannot be assumed zero. Nevertheless, if the Mach number just upstream of the shock is close to 1 then the shock is said to be 'weak' and it may be shown that $\Delta S \sim (M-1)^3$. This is why transonic flows are traditionally studied based on the potential flow theory. In this approach the thickness of the aerofoil δ is supposed small and the solution is represented by asymptotic expansions (2.41)–(2.43). It may be easily seen from (2.42) and (2.43) that everywhere in the flow field $M - 1 \sim \delta^{2/3}$.

Thus not only the leading-order perturbation, which in the asymptotic expansion (2.41) of the potential is represented by $\delta^{2/3}\phi_0(x,\tilde{y})$, but also the next-order term $\delta^{4/3}\phi_1(x,\tilde{y})$ may be treated based on the potential flow theory.

The analysis in §§ 2.1 and 2.3 does not rely on the assumption that the aerofoil thickness is small. Therefore an alternative justification of the irrotational character of the flow near the separation point is needed. Similarly to (2.16) we write the velocity vector $\boldsymbol{V}$, vorticity $\boldsymbol{\omega}$, temperature T and entropy S in form of the asymptotic expansions

$$\left.\begin{aligned} &\boldsymbol{V} = \boldsymbol{V}_0(x,y) + \epsilon\boldsymbol{V}_1(x,y) + \cdots, \quad \boldsymbol{\omega} = \boldsymbol{\omega}_0(x,y) + \epsilon\boldsymbol{\omega}(x,y) + \cdots, \\ &T = T_0(x,y) + \epsilon T_1(x,y) + \cdots, \quad S = S_0(x,y) + \epsilon S_1(x,y) + \cdots. \end{aligned}\right\} \tag{A 4}$$

Substitution of (A 4) into (A 1) yields

$$\boldsymbol{V}_0 \times \boldsymbol{\omega}_0 = T_0 \nabla S_0, \tag{A 5}$$

$$\boldsymbol{V}_0 \times \boldsymbol{\omega}_1 = T_0 \nabla S_1 + T_1 \nabla S_0 - \boldsymbol{V}_1 \times \boldsymbol{\omega}_0. \tag{A 6}$$

If the body shape at the location of the shock is smooth then S_0 appears to be a regular function everywhere downstream of the shock. This means that the right-hand side of equation (A 5) is finite. At the same time, it follows from (2.26), (2.27) that

$$\boldsymbol{\omega}_0 = \boldsymbol{e}\left(\frac{\partial u_0}{\partial y} - \frac{\partial v_0}{\partial x}\right) = \boldsymbol{e}\, y^{-3/5}\,\Omega_0(\xi) + \cdots \quad \text{as} \quad y \to 0, \tag{A 7}$$

where $\boldsymbol{e}$ is a unit vector normal to the (x,y)-plane. Substitution of (2.26), (2.27) and (A 7) into (A 5) yields $\Omega_0(\xi) = 0$.

Similarly from (2.73) it follows that $\boldsymbol{\omega}_1$ also is singular, i.e.

$$\boldsymbol{\omega}_1 = \boldsymbol{e}\, y^{-1}\,\Omega_1(\xi) + \cdots \quad \text{as} \quad y \to 0,$$

whence using (A 6) we can conclude that $\Omega_1(\xi) = 0$. This confirms that the leading- and first-order terms in asymptotic expansions (2.16) may be studied based on the potential flow theory.

Appendix B

Here we shall consider the process of interaction between the boundary layer and inviscid flow using the 'inspection analysis' (see Sychev *et al.* 1998). Let $U_{00}(Y)$ be the distribution of velocity across the boundary layer immediately upstream of the interaction region. We shall suppose that

$$U_{00}(Y) = AY^{1/m} + \cdots \quad \text{as} \quad Y \to 0, \tag{B 1}$$

with m being a positive constant. Let us further suppose that there is a small pressure variation Δp along the body surface acting upon the boundary layer over a small distance Δx. It is apparent that the pressure rise/decay will result in a deceleration/acceleration of fluid particles inside the boundary layer. To estimate the corresponding velocity variation Δu one needs to compare the convective term in the longitudinal momentum equation with the pressure gradient

$$u\frac{\partial u}{\partial x} \sim \frac{\partial p}{\partial x}. \tag{B 2}$$

Equation (B 2) may be also written as

$$u\frac{\Delta u}{\Delta x} \sim \frac{\Delta p}{\Delta x},$$

and it follows that

$$\Delta u \sim \frac{\Delta p}{u}. \tag{B 3}$$

In the main part of the boundary layer $u = O(1)$, and it follows from (B 3) that

$$\Delta u \sim \Delta p.$$

If now we consider a small filament in the main part of the boundary layer confined between two neighbouring streamlines with δ being the initial distance between them, then using the mass conservation law it is easy to see that this distance will change by the value

$$\Delta\delta \sim \delta\Delta u \sim \delta\Delta p.$$

The integral effect of all the filaments in the main part of the boundary layer may be estimated as

$$\Delta\delta \sim Re^{-1/2}\Delta p. \tag{B 4}$$

The above analysis is obviously invalid near the bottom of the boundary layer where the velocity u is as small as its perturbation Δu. In this new region occupying a thin sublayer near the wall, equation (B 3) yields

$$u \sim \Delta u \sim \sqrt{\Delta p}. \tag{B 5}$$

Comparing (B 5) with (B 1) we can find that

$$\sqrt{\Delta p} \sim Y^{1/m},$$

which being solved for Y gives the following estimate for the thickness of the sublayer:

$$y \sim Re^{-1/2}Y \sim Re^{-1/2}(\Delta p)^{m/2}. \tag{B 6}$$

To estimate the displacement effect of the sublayer we again use the mass conservation law. Treating the sublayer as one filament and taking into account that inside this filament $\Delta u \sim u$ we have to conclude that the variation of the filament thickness is of the same order as its initial value given by (B 6), i.e.

$$\Delta\delta \sim Re^{-1/2}(\Delta p)^{m/2}. \tag{B 7}$$

Comparing (B 7) with (B 4) we see that the contribution of the sublayer to the displacement effect of the boundary layer is comparable with that of the main part of the boundary layer provided that $m = 2$.

REFERENCES

Abramowitz, M. & Stregun, I. A. 1965 *Handbook of Mathematical Functions*, 3rd Edn. Dover.

Ackerberg, R. C. 1970 Boundary-layer separation at free streamline. Part 1. Two-dimensional flow. *J. Fluid Mech.* **44**, 211–225.

Ackerberg, R. C. 1971 Boundary-layer separation at free streamline. Part 2. Numerical results. *J. Fluid Mech.* **46**, 727–736.

Bodonyi, R. J. 1979 Transonic laminar boundary-layer flow near convex corners. *Q. J. Mech. Appl. Maths* **32**, 63–71.

Bodonyi, R. J. & Kluwick, A. 1977 Freely interacting transonic boundary layers. *Phys. Fluids* **20**, 1432–1437.

Bodonyi, R. J. & Kluwick, A. 1982 Supercritical transonic trailing-edge flow. *Q. J. Mech. Appl. Maths* **35**, 265–277.

Bodonyi, R. J. & Kluwick, A. 1998 Transonic trailing-edge flow. *Q. J. Mech. Appl. Maths* **51**, 297–310.

Brown, S. N., Cheng, H. K. & Lee, C. J. 1990 Inviscid-viscous interaction on triple-deck scales in a hypersonic flow with strong wall cooling. *J. Fluid Mech.* **220**, 309–337.

Cole, J. D. & Cook, L. P. 1986 *Transonic Aerodynamics*. North-Holland.

Diesperov, V. N. 1981 The structure of the boundary layer for transonic flow around a convex corner with a free streamline. *Dokl. Akad. Nauk SSSR* **257**, 1314–1318.

Diesperov, V. N. 1983 Boundary layer with self-induced pressure in transonic flow over a corner point of an aerofoil. *Dokl. Akad. Nauk SSSR* **271**, 562–566.

Diesperov, V. N. 1994 Some solutions of Kármán's equation describing the transonic flow a corner point on an aerofoil with a curvilinear generatrix. *Prilk. Mat. Mekh.* **58**(6), 68–77.

Falkovich, S. V. & Chernov, I. A. 1964 Flow of a sonic gas stream past a body of revolution. *Prikl. Math. Mech.* **28**, 280–284.

Guderley, K. G. 1962 *The Theory of Transonic Flow*, 1st Edn. Pergamon.

Guderley, K. G. & Yoshihara, H. 1951 An axial-symmetric transonic flow pattern. *Q. Appl. Maths* **8**, 333–339.

Kerimbekov, R. M., Ruban, A. I. & Walker, J. D. A. 1994 Hypersonic boundary-layer separation on a cold wall. *J. Fluid Mech.* **274**, 163–195.

Messiter, A. F. 1970 Boundary-layer flow near the trailing edge of a flat plate. *SIAM J. Appl. Maths* **18**, 241–257.

Messiter, A. F. & Liñáñ, A. 1976 The vertical plate in laminar free convection: Effects of leading and trailing edges and discontinuous temperature. *Z. Angew. Math. Phys.* **27**, 633–651.

Messiter, A. F., Matarrese, M. D. & Adamson, T. C. 1991 Strip blowing from a wedge at hypersonic speeds. *AIAA Paper* 91-0032.

Neiland, V. Y. 1969 Theory of laminar boundary layer separation in supersonic flow. *Izv. Akad. Nauk SSSR, Mech. Zhidk. Gaza*, part 4, 53–57.

Neiland, V. Y. 1973 Peculiarities of boundary-layer separation on a cooled body and its interaction with a hypersonic flow. *Izv. Akad. Nauk SSSR, Mech. Zhidk. Gaza*, part 6, 99–109.

Neiland, V. Y. & Sokolov, L. A. 1975 On the asymptotic theory of incipient separation in compression ramp hypersonic flow on cooled body for a weak hypersonic interaction regime. *Uch. Zap. TsAGI* **6**(3), 25–34.

Oleinik, O. A. & Samohin, V. N. 1997 *Mathematical Methods in Boundary-Layer Theory*. Nauka, Moscow.

Pearson, H., Holliday, J. B. & Smith, S. F. 1958 A theory of the cylindrical ejector supersonic propelling nozzle. *J. Aeronaut. Soc.* **62**, 756–761.

Ruban, A. I. 1974 On laminar separation from a corner point on a solid surface. *Uch. Zap. TsAGI* **5**(2), 44–54.

Shidlovskii, V. P. 1977 The structure of the viscous fluid flow near the edge of a rotating disk. *Prikl. Mat. Mekh.* **41**(3), 464–472.

Smith, F. T. & Duck, P. W. 1977 Separation of jets or thermal boundary layers from a wall. *Q. J. Mech. Appl. Maths* **30**, 143–156.

Stewartson, K. & Williams, P. G. 1969 Self-induced separation. *Proc. R. Soc. Lond.* A **312**, 181–206.

Sychev, V. V., Ruban, A. I., Sychev, Vic. V. & Korolev, G. L. 1998 *Asymptotic Theory of Separated Flows*. Cambridge University Press.